Chance Constrained Scheduling and Pricing for Multi-Service Battery Energy Storage

Weifeng Zhong, Kan Xie, Yi Liu, Shengli Xie, *Fellow, IEEE*, and Lihua Xie, *Fellow, IEEE*

***Abstract*—This paper studies optimal day-ahead scheduling of grid-connected batteries that simultaneously provide three services: 1) load shifting, 2) real-time balancing, and 3) primary frequency control (PFC). The uncertainties of load and frequency are incorporated in the cost-minimizing scheduling problem via chance constraints. The resulting chance-constrained problem is then reformulated into a mixed-integer second-order cone program (MISOCP) that can be solved by commercial solvers. However, it is computationally formidable to obtain the globally optimal solution to the MISOCP due to the big problem size. To obtain a suboptimal solution quickly, a heuristic based on penalty alternating direction method (PADM) is developed to solve the MISOCP. Fixing the integer solution returned by the heuristic, we adopt the duality of the second-order cone program (SOCP) to price the three services in the local market. Theoretical analysis of the market equilibrium, individual rationality, and balanced budget is given. Real-world data of load, frequency, and price in the French grid is used in simulation. The results show that the proposed heuristic is computationally efficient, and the pricing results can guarantee a positive utility for each of the batteries, incentivizing them to provide services.**

***Index Terms*—Chance constraints, battery energy storage, multi-service battery, primary frequency control, pricing.**

Manuscript received April 16, 2021; revised July 7, 2021; accepted August 16, 2021. Date of publication August 31, 2021; date of current version October 21, 2021. This work was supported in part by the National Natural Science Foundation of China under Grant 62003099, Grant 61973087, and Grant U1911401; in part by the National Key R&D Program of China under Grant 2020YFB1807805 and Grant 2020YFB1807800; and in part by the State Key Laboratory of Synthetical Automation for Process Industries under Grant 2020-KF-21-02. Paper no. TSG-00592-2021. *(Corresponding author: Yi Liu.)*

Weifeng Zhong is with the School of Automation, Guangdong University of Technology, Guangzhou 510006, China, and also with the Guangdong Key Laboratory of IoT Information Technology, Guangzhou 510006, China (e-mail: wfzhongs@gdut.edu.cn).

Kan Xie is with the School of Automation, Guangdong University of Technology, Guangzhou 510006, China, and also with the Key Laboratory of Intelligent Detection and Internet of Things in Manufacturing, Ministry of Education, Guangzhou 510006, China (e-mail: kxie@gdut.edu.cn).

Yi Liu is with the School of Automation, Guangdong University of Technology, Guangzhou 510006, China, and also with the Guangdong–Hong Kong–Macao Joint Laboratory for Smart Discrete Manufacturing, Guangzhou 510006, China (e-mail: yi.liu@gdut.edu.cn).

Shengli Xie is with the School of Automation, Guangdong University of Technology, Guangzhou 510006, China, and also with the 111 Center for Intelligent Batch Manufacturing Based on IoT Technology, Guangzhou 510006, China (e-mail: shlxie@gdut.edu.cn).

Lihua Xie is with the School of Electrical and Electronic Engineering, Nanyang Technological University, Singapore 639798 (e-mail: elhxie@ntu.edu.sg).

Color versions of one or more figures in this article are available at https://doi.org/10.1109/TSG.2021.3109140.

Digital Object Identifier 10.1109/TSG.2021.3109140

NOMENCLATURE

Indices and Sets

$i, \boldsymbol{I}$	Index and set of batteries, $i \in \boldsymbol{I}$.
k	Index of frequency time slots.
n	Index of discharging or charging, $n \in \{\mathtt{d}, \mathtt{c}\}$.
$t, \boldsymbol{T}$	Index and set of time periods, $t \in \boldsymbol{T}$.

Parameters

$\boldsymbol{e}$	Vector that includes all uncertainties in the system.
Δf_k	Frequency deviation in slot k (Hz).
Δk	Length of a frequency time slot (s).
Δt	Length of a time period (h).
$\epsilon_{\mathtt{p}}, \epsilon_{\mathtt{s}}$	Safety parameter for battery power/capacity.
$\eta_i^{\mathtt{d}}, \eta_i^{\mathtt{c}}$	Discharging/charging efficiency of battery i.
$\sigma_{\mathtt{D},t}$	Standard deviation of $e_{\mathtt{D},t}$ (kWh).
$\sigma_{\mathtt{W},t}$	Standard deviation of $e_{\mathtt{W},t}$ (kWh).
σ_n	Standard deviation of e_n (h).
ξ_n	Equivalent discharging/charging time of a battery that provides PFC in a time period (h), where $n \in \{\mathtt{d}, \mathtt{c}\}$.
D_t	Predicted energy consumption in time t (kWh).
$e_{\mathtt{D},t}$	Random variable denoting the uncertainty of energy consumption in time t (kWh).
$e_{\mathtt{W},t}$	Random variable denoting the uncertainty of RES energy generation in time t (kWh).
E_n	Predicted value (i.e., mean) of ξ_n (h).
e_n	Random variable denoting the uncertainty of ξ_n (h).
$f_{\mathtt{db}}$	Deadband for PFC (Hz).
$f_{\mathtt{max}}$	Full activation frequency deviation for PFC (Hz).
$P_i^{\mathtt{max}}$	Maximum discharging/charging power of battery i (kW).
$Q_t^{\mathtt{b}}$	Price at which energy is bought from the grid in time t (\$/kWh).
$Q_t^{\mathtt{s}}$	Price at which energy is sold to the grid in time t (\$/kWh).
$Q_{\mathtt{m}}$	Price of committed power for PFC (\$/kW).
$S_i^{\mathtt{max}}$	Maximum energy state of battery i (kWh).
$S_i^{\mathtt{min}}$	Minimum energy state of battery i (kWh).
W_t	Predicted RES energy generation in time t (kWh).

Variables

$\vartheta_{n,i}(\cdot)$	Discharging/charging cost function of battery i (\$), where $n \in \{\mathtt{d}, \mathtt{c}\}$.
$a_{i,t}^n$	Participation factor of the discharging/charging power of battery i for balancing in time t, where $n \in \{\mathtt{d}, \mathtt{c}\}$.
$g_t^{\mathtt{b}}$	Energy bought from the grid in time t (kWh).

$g_t^{\mathtt{s}}$ Energy sold to the grid in time t (kWh).
$p_{i,t}^n$ Discharging/charging power of battery i for load shifting in time t (kW), where $n \in \{\mathtt{d}, \mathtt{c}\}$.
$p_{i,t}^n(\boldsymbol{e})$ Discharging/charging power of battery i for load shifting and balancing in time t (kW), where $n \in \{\mathtt{d}, \mathtt{c}\}$.
$r_{i,t}^n$ Discharging/charging power of battery i for PFC in time t (kW), where $n \in \{\mathtt{d}, \mathtt{c}\}$.
r_k Actual power for PFC in slot k (kW).
$r_{\mathtt{m}}$ Committed power for PFC (kW).
$s_{i,t}(\boldsymbol{e})$ Energy stored in battery i in time t considering uncertainty $\boldsymbol{e}$ (kWh).
$x_{i,t}^n$ Binary variable indicating the discharging/charging state of battery i in time t, where $n \in \{\mathtt{d}, \mathtt{c}\}$.

I. Introduction

BATTERY energy storage characterized by high ramp rates and fast response can provide power systems with multiple services such as 1) *load shifting* [1]: move energy consumption and generation across time periods to prevent network overload, reduce generation cost, and realize energy arbitrage; 2) *real-time balancing* [2], [3]: offset unforeseen real-time variations of consumption and generation to achieve demand-supply balance; 3) *frequency control* [4]: respond to fast frequency deviations for maintaining power quality and system stability. In deregulated electricity markets, battery operators would optimize the use of charging and discharging power in multiple services to maximize revenue [5]. Via appropriate market and pricing rules, battery operators could be incentivized to increase investment in high-performance batteries. This will greatly benefit power systems in transitioning to massive use of distributed, intermittent renewable energy sources (RES) and minimum use of controllable thermal generation.

This paper studies optimal day-ahead scheduling and pricing for grid-connected batteries that simultaneously provide three services: 1) load shifting, 2) real-time balancing, and 3) primary frequency control (PFC). The comparison with the related works is summarized in Table I. Load shifting is the most common battery service based on the foreseeable demand and RES supply. In contrast, balancing and frequency control require that part of battery power is reserved for responding to real-time uncertain variations. In [8]–[11], power reserve decisions are made based on the upper and lower bounds of uncertainty. Their reserve results are mostly conservative, leading to relatively high system costs. Another flexible way to handle uncertainty is to employ distributionally robust chance constraints [2], [12]–[14], which have been increasingly used in recent related works. Chance constraints are characterized by the statistical information of uncertainty. Adjusting the safety parameters in chance constraints can strike a balance between reliability and economy [15]. In addition, most related works [2], [6]–[14] focus on the scheduling for multi-service batteries from a system-wide view but lack discussion on profit allocation among multiple batteries that jointly provide services. In this paper, we propose a pricing method for a local market, which can quantify each battery's income from each service and incentivize batteries to provide services.

The technical contributions of this paper are as follows.

- We propose a chance-constrained model of batteries incorporating load shifting, balancing, and PFC. In particular, empirical information of means and variances is derived from real-world frequency deviation data, characterizing the uncertainty of energy content in PFC.
- We reformulate the chance-constrained multi-service scheduling problem to a mixed-integer second-order cone program (MISOCP) that can be solved by off-the-shelf solvers. However, getting the globally optimal solution is badly time-consuming due to the big problem size. We thus develop a heuristic based on penalty alternating direction method (PADM) [16] to solve the MISOCP. The results show that the proposed heuristic can obtain high-quality feasible solutions quickly.
- By fixing the integer solution returned by the heuristic, the MISOCP becomes a second-order cone program (SOCP). We then employ the duality of the SOCP to price the three services in the local market. We also provide theoretical analysis of market equilibrium, individual rationality, and balanced budget. The pricing results show that each battery has a positive utility, i.e., service incomes are enough to cover battery costs.

The novelty of this paper is twofold. 1) We consider multi-period scheduling for batteries to provide three services, which leads to a large-size mixed-integer problem, and then we newly employ PADM as a heuristic to efficiently solve the problem. 2) We use the duality-based pricing method to determine the profit allocation among batteries that cooperatively provide multiple services. These two points are the major differences compared with the existing works on multi-service energy storage, e.g., [2], [6]–[14].

II. System Model

Consider a local system (e.g., a microgrid) consisting of consumers, RES, and batteries. Each battery is indexed by $i \in \boldsymbol{I} \coloneqq \{1, \ldots, I\}$. The scheduling horizon is the next operating day which is divided into multiple time periods, and each period is indexed by $t \in \boldsymbol{T} \coloneqq \{1, \ldots, T\}$. Let W_t be the predicted total energy (kWh) produced by RES and D_t be the predicted total energy consumption (kWh) in t. We call $(D_t - W_t)$ the (net) *load* of the system in t. Suppose that the load and batteries are connected to a bus without considering line flow limits. The data interaction among different entities can be implemented by advanced communications and computing technologies [17], [18]. In what follows, we introduce the three battery services and the chance-constrained battery model.

A. Load Shifting

Let $p_{i,t}^{\mathtt{d}}$ and $p_{i,t}^{\mathtt{c}}$ denote the discharging and charging power (kW) of battery i in t, respectively. Let $g_t^{\mathtt{b}}$ and $g_t^{\mathtt{s}}$ be the energy (kWh) that the system buys from and sells to the grid, respectively. The energy balance of the system for $t \in \boldsymbol{T}$ is

TABLE I
RELATED WORKS ON MULTI-SERVICE ENERGY STORAGE

Ref.	Load shifting	Balancing	Frequency control	Service pricing	Uncertainty representation	Uncertainty handling
[6]	✓	-	✓	-	-	Model predictive control
[7]	✓	✓	✓	-	-	Fixed energy margins
[8]	-	✓	✓	-	Upper and lower bounds	-
[9]	✓	-	✓	-	Upper and lower bounds	Lyapunov optimization
[10], [11]	✓	✓	-	-	Upper and lower bounds	Robust counterparts
[2], [12]–[14]	✓	✓	-	-	Means and (co)variances	Chance constraints
This paper	✓	✓	✓	✓	Means and (co)variances	Chance constraints

described by

$$\sum_{i\in\boldsymbol{I}}\left(p^{\mathrm{d}}_{i,t}-p^{\mathrm{c}}_{i,t}\right)+g^{\mathrm{b}}_t-g^{\mathrm{s}}_t=D_t-W_t, \tag{1}$$

$$p^{\mathrm{d}}_{i,t}\geq 0,\quad p^{\mathrm{c}}_{i,t}\geq 0,\quad g^{\mathrm{b}}_t\geq 0,\quad g^{\mathrm{s}}_t\geq 0. \tag{2}$$

In this paper, we set the length of a time period to $\Delta t=1$ h, so Δt is omitted in the first term in (1). The first battery service is to shift the system's load among periods in order to reduce the cost in trading energy with the grid. For this service, the decision variables are $\boldsymbol{g}\coloneqq\{g^{\mathrm{b}}_t,g^{\mathrm{s}}_t\}_{t\in\boldsymbol{T}}$ and $\boldsymbol{p}\coloneqq\{\boldsymbol{p}_i\}_{i\in\boldsymbol{I}}$ where $\boldsymbol{p}_i\coloneqq\{p^{\mathrm{d}}_{i,t},p^{\mathrm{c}}_{i,t}\}_{t\in\boldsymbol{T}}$.

B. Real-Time Balancing

D_t and W_t are predictive values that are rarely equal to their actual measurements. Define $e_{\mathrm{D},t}$ as a random variable representing the consumption uncertainty (kWh) with a mean of $\mathrm{E}[e_{\mathrm{D},t}]=0$ and a variance of $\mathrm{Var}[e_{\mathrm{D},t}]=\sigma^2_{\mathrm{D},t}$. Similarly, let $e_{\mathrm{W},t}$ stand for the RES uncertainty with $\mathrm{E}[e_{\mathrm{W},t}]=0$ and $\mathrm{Var}[e_{\mathrm{W},t}]=\sigma^2_{\mathrm{W},t}$. Let $\boldsymbol{e}$ be a vector representing all the uncertainties in the system. Let $p^{\mathrm{d}}_{i,t}(\boldsymbol{e})$ and $p^{\mathrm{c}}_{i,t}(\boldsymbol{e})$ denote the discharging and charging power under uncertainty $\boldsymbol{e}$, respectively. The energy balance under uncertainty for $t\in\boldsymbol{T}$ is described by

$$\sum_{i\in\boldsymbol{I}}\left[p^{\mathrm{d}}_{i,t}(\boldsymbol{e})-p^{\mathrm{c}}_{i,t}(\boldsymbol{e})\right]+g^{\mathrm{b}}_t-g^{\mathrm{s}}_t=D_t+e_{\mathrm{D},t}-\left(W_t+e_{\mathrm{W},t}\right), \tag{3}$$

$$p^{\mathrm{d}}_{i,t}(\boldsymbol{e})=p^{\mathrm{d}}_{i,t}+a^{\mathrm{d}}_{i,t}\left(e_{\mathrm{D},t}-e_{\mathrm{W},t}\right), \tag{4}$$

$$p^{\mathrm{c}}_{i,t}(\boldsymbol{e})=p^{\mathrm{c}}_{i,t}-a^{\mathrm{c}}_{i,t}\left(e_{\mathrm{D},t}-e_{\mathrm{W},t}\right). \tag{5}$$

In (4) and (5), $\{p^{\mathrm{d}}_{i,t},p^{\mathrm{c}}_{i,t}\}$ are scheduled values, and $\{a^{\mathrm{d}}_{i,t},a^{\mathrm{c}}_{i,t}\}$ are the participation factors of battery i in t. A higher $a^{\mathrm{d}}_{i,t}$ (or $a^{\mathrm{c}}_{i,t}$) means that battery i reserves more discharging (or charging) power for load uncertainty $(e_{\mathrm{D},t}-e_{\mathrm{W},t})$. We define

$$\sum_{i\in\boldsymbol{I}}\left(a^{\mathrm{d}}_{i,t}+a^{\mathrm{c}}_{i,t}\right)=1, \tag{6}$$

$$a^{\mathrm{d}}_{i,t}\geq 0,\quad a^{\mathrm{c}}_{i,t}\geq 0. \tag{7}$$

The second battery service is to reserve batteries' power to offset the realization of load uncertainty. The corresponding decision variables are $\boldsymbol{a}\coloneqq\{\boldsymbol{a}_i\}_{i\in\boldsymbol{I}}$ where $\boldsymbol{a}_i\coloneqq\{a^{\mathrm{d}}_{i,t},a^{\mathrm{c}}_{i,t}\}_{t\in\boldsymbol{T}}$. Once $\{\boldsymbol{p},\boldsymbol{a}\}$ are determined and the realization of $(e_{\mathrm{D},t}-e_{\mathrm{W},t})$ is known, the actual battery operation on the operating day can be directly provided by (4) and (5).

C. Primary Frequency Control (PFC)

The third battery service is to provide the grid with PFC. Let $r_{\mathrm{m}}\geq 0$ be the power (kW) committed by the local system for PFC. Once r_{m} is determined, the system should ensure that $\pm r_{\mathrm{m}}$ is always available for all periods $t\in\boldsymbol{T}$ on the operating day. The committed power $\pm r_{\mathrm{m}}$ is jointly provided by multiple batteries. Let $r^{\mathrm{d}}_{i,t}$ and $r^{\mathrm{c}}_{i,t}$ denote the discharging and charging power (kW) committed by battery i for PFC in t, respectively. We have

$$\sum_{i\in\boldsymbol{I}}r^{\mathrm{d}}_{i,t}=r_{\mathrm{m}},\quad \sum_{i\in\boldsymbol{I}}r^{\mathrm{c}}_{i,t}=r_{\mathrm{m}}, \tag{8}$$

$$r_{\mathrm{m}}\geq 0,\quad r^{\mathrm{d}}_{i,t}\geq 0,\quad r^{\mathrm{c}}_{i,t}\geq 0. \tag{9}$$

The decision variables for PFC are $\boldsymbol{r}\coloneqq\{r_{\mathrm{m}},\{\boldsymbol{r}_i\}_{i\in\boldsymbol{I}}\}$ where $\boldsymbol{r}_i\coloneqq\{r^{\mathrm{d}}_{i,t},r^{\mathrm{c}}_{i,t}\}_{t\in\boldsymbol{T}}$. Note that $\boldsymbol{r}$ denotes the committed (maximum) power. On the operating day, the actual power for PFC will vary according to real-time frequency deviation.

Next, we model the uncertainty of PFC in the time domain. A frequency time slot is indexed by k. The length of a frequency time slot is denoted by Δk (e.g., 10 s) that is much shorter than the length of a time period $\Delta t=1$ h. The frequency deviation (Hz) is given by $\Delta f_k=f_{\mathrm{N}}-f_k$ where f_{N} is the nominal frequency (e.g., 50 Hz) and f_k is the local frequency measured at time slot k. Put aside the batteries indexed by $i\in\boldsymbol{I}$ temporarily and consider a conceptual battery that fully provides the committed power $\pm r_{\mathrm{m}}$. Define r_k as the actual power of the conceptual battery responding to frequency deviation Δf_k with $-r_{\mathrm{m}}\leq r_k\leq r_{\mathrm{m}}$. Following the proportional rule of PFC [4], we have

$$r_k=\begin{cases}0, & \text{if } |\Delta f_k|\leq f_{\mathtt{db}};\\ r_{\mathrm{m}}(\Delta f_k/f_{\mathtt{max}}), & \text{if } f_{\mathtt{db}}<|\Delta f_k|\leq f_{\mathtt{max}};\\ r_{\mathrm{m}}(\Delta f_k/|\Delta f_k|), & \text{if } |\Delta f_k|>f_{\mathtt{max}}.\end{cases} \tag{10}$$

In the first case in (10), $f_{\mathtt{db}}\geq 0$ denotes the deadband. Any frequency deviation within the deadband will not be responded. In the second case, $f_{\mathtt{max}}>0$ denotes the full activation frequency deviation, and r_k is proportional to Δf_k. In the third case, r_k is at its maximum or minimum, $\pm r_{\mathrm{m}}$. Here, $\{f_{\mathtt{db}},f_{\mathtt{max}}\}$ are fixed parameters that are generally decided by the grid. The grid could also provide several choices of $\{f_{\mathtt{db}},f_{\mathtt{max}}\}$, and the local system chooses one of them.

By the second and third cases in (10), it can be seen that the conceptual battery is discharged ($r_k>0$) if $\Delta f_k>0$, and it is charged ($r_k<0$) if $\Delta f_k<0$. In a period of Δt , we define two sets of time slots: $\boldsymbol{K}^{\mathrm{d}}_1=\{k\mid f_{\mathtt{db}}<\Delta f_k\leq f_{\mathtt{max}}\}$ and $\boldsymbol{K}^{\mathrm{d}}_2=\{k\mid \Delta f_k>f_{\mathtt{max}}\}$. These two sets are composed of

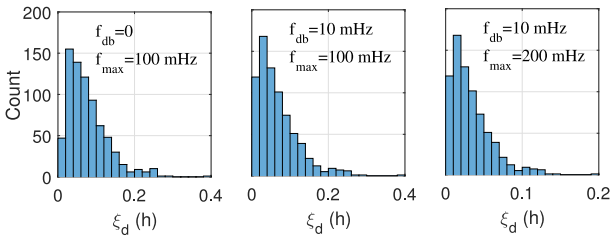

Fig. 1. Histograms of the equivalent discharging time $\xi_{\mathtt{d}}$. Δf_k is given by the 10-second frequency deviation data ($\Delta k = 10$ s) measured during Dec. 2019 in the French grid [19].

the time slots at which the battery is discharged. According to (10), the discharging energy (kWh) in Δt is denoted by

$$\begin{aligned}\sum_{k\in\boldsymbol{K}_1^{\mathtt{d}}\cup\boldsymbol{K}_2^{\mathtt{d}}} r_k\Delta k &= \sum_{k\in\boldsymbol{K}_1^{\mathtt{d}}} r_{\mathtt{m}}\frac{\Delta f_k}{f_{\max}}\Delta k + \left|\boldsymbol{K}_2^{\mathtt{d}}\right| r_{\mathtt{m}}\Delta k \\ &= r_{\mathtt{m}}\Delta k\left(\sum_{k\in\boldsymbol{K}_1^{\mathtt{d}}}\frac{\Delta f_k}{f_{\max}} + \left|\boldsymbol{K}_2^{\mathtt{d}}\right|\right) \\ &= r_{\mathtt{m}}\xi_{\mathtt{d}}, \end{aligned} \tag{11}$$

where $\xi_{\mathtt{d}}$ is called *the equivalent discharging time* (h) of a battery that provides PFC in Δt. By (11), the uncertainty in PFC is transferred from r_k to $\xi_{\mathtt{d}}$ that is in the time domain. Similarly, if battery i has a committed discharging power of $r_{i,t}^{\mathtt{d}}$ in time period t, its discharging energy caused by PFC is $r_{i,t}^{\mathtt{d}}\xi_{\mathtt{d}}$. Following the same way, we can define *the equivalent charging time* $\xi_{\mathtt{c}}$.

According to the definition in (11), $\xi_{\mathtt{d}}$ is determined by predefined parameters $\{\Delta k, f_{\mathtt{db}}, f_{\max}\}$ and uncertain deviations Δf_k. Here, we consider $\xi_{\mathtt{d}}$ as a random variable with $\mathrm{E}[\xi_{\mathtt{d}}] = E_{\mathtt{d}}$ and $\mathrm{Var}[\xi_{\mathtt{d}}] = \sigma_{\mathtt{d}}^2$. Fig. 1 shows the histograms of $\xi_{\mathtt{d}}$ [19]. Let $\xi_{\mathtt{d}} = E_{\mathtt{d}} + e_{\mathtt{d}}$ where $e_{\mathtt{d}}$ represents the uncertainty of $\xi_{\mathtt{d}}$ with $\mathrm{E}[e_{\mathtt{d}}] = 0$ and $\mathrm{Var}[e_{\mathtt{d}}] = \sigma_{\mathtt{d}}^2$. Hereafter, we use $\{E_{\mathtt{d}}, e_{\mathtt{d}}\}$ instead of $\xi_{\mathtt{d}}$. Similarly, we define $E_{\mathtt{c}}$ as the mean of $\xi_{\mathtt{c}}$ and $e_{\mathtt{c}}$ as the corresponding uncertainty with $\mathrm{E}[e_{\mathtt{c}}] = 0$ and $\mathrm{Var}[e_{\mathtt{c}}] = \sigma_{\mathtt{c}}^2$. In simulation, $\{E_{\mathtt{d}}, E_{\mathtt{c}}, \sigma_{\mathtt{d}}^2, \sigma_{\mathtt{c}}^2\}$ are sampling values derived from the French grid data [19]. Now, we have $r_{i,t}^{\mathtt{d}}(E_{\mathtt{d}} + e_{\mathtt{d}})$ and $r_{i,t}^{\mathtt{c}}(E_{\mathtt{c}} + e_{\mathtt{c}})$, which denote the ith battery's discharging and charging energy (kWh) caused by PFC in time period t, respectively. These two terms relate to battery energy state evolution and operating cost, which will be presented in the following sections. In this paper, the uncertainty of PFC is described by $\{e_{\mathtt{d}}, e_{\mathtt{c}}\}$.

D. Chance-Constrained Battery Model

The system uncertainty vector can be formally defined as $\boldsymbol{e} \coloneqq \{\{e_{\mathtt{D},t}, e_{\mathtt{W},t}\}_{t\in\boldsymbol{T}}, e_{\mathtt{d}}, e_{\mathtt{c}}\}$ including the uncertainties of demand, RES, and PFC. Let $\eta_i^{\mathtt{d}}$ and $\eta_i^{\mathtt{c}}$ be the discharging and charging efficiencies of battery i, respectively. Define $s_{i,t}(\boldsymbol{e})$ as the energy (kWh) stored in battery i in t under uncertainty $\boldsymbol{e}$. The energy state evolution of battery i is given by

$$s_{i,t+1}(\boldsymbol{e}) = s_{i,1} + \sum_{\tau=1}^{t}\left[\eta_i^{\mathtt{c}} p_{i,\tau}^{\mathtt{c}}(\boldsymbol{e}) - \frac{1}{\eta_i^{\mathtt{d}}} p_{i,\tau}^{\mathtt{d}}(\boldsymbol{e})\right]$$

$$+ \sum_{\tau=1}^{t}\left[\eta_i^{\mathtt{c}} r_{i,\tau}^{\mathtt{c}}(E_{\mathtt{c}} + e_{\mathtt{c}}) - \frac{1}{\eta_i^{\mathtt{d}}} r_{i,\tau}^{\mathtt{d}}(E_{\mathtt{d}} + e_{\mathtt{d}})\right], \tag{12}$$

where the first square bracket denotes the energy change caused by load shifting and balancing, and the second square bracket is the energy change caused by PFC.

Next, we define the chance constraints for $p_{i,t}^{\mathtt{d}}(\boldsymbol{e})$, $p_{i,t}^{\mathtt{c}}(\boldsymbol{e})$, and $s_{i,t+1}(\boldsymbol{e})$. Without assuming that $\boldsymbol{e}$ follows a certain distribution, we consider that the underlying distribution of $\boldsymbol{e}$ comes from a family of distributions (i.e., an ambiguity set) that share the same mean and covariance matrix [15]. According to (4) and (5), we define a random vector $\boldsymbol{e}_{\mathtt{p},t} \coloneqq \{e_{\mathtt{D},t}, e_{\mathtt{W},t}\}$ representing the uncertainty relating to $\{p_{i,t}^{\mathtt{d}}(\boldsymbol{e}), p_{i,t}^{\mathtt{c}}(\boldsymbol{e})\}$. Let $\Sigma_{\mathtt{p},t}$ be the covariance matrix of $\boldsymbol{e}_{\mathtt{p},t}$. The ambiguity set for $\boldsymbol{e}_{\mathtt{p},t}$ is defined as

$$\Omega_{\mathtt{p},t} \coloneqq \left\{\mathbb{P} \mid \mathrm{E}_{\mathbb{P}}\left[\boldsymbol{e}_{\mathtt{p},t}\right] = \boldsymbol{0}, \mathrm{E}_{\mathbb{P}}\left[\boldsymbol{e}_{\mathtt{p},t}\boldsymbol{e}_{\mathtt{p},t}^{\top}\right] = \Sigma_{\mathtt{p},t}\right\}, \tag{13}$$

where $\mathbb{P}$ stands for a probability distribution/function. The chance constraints for discharging and charging power of battery $i \in \boldsymbol{I}$ in $t \in \boldsymbol{T}$ are written as

$$\inf_{\mathbb{P}\in\Omega_{\mathtt{p},t}} \mathbb{P}\left[0 \le p_{i,t}^{\mathtt{d}}(\boldsymbol{e}) + r_{i,t}^{\mathtt{d}} \le x_{i,t}^{\mathtt{d}} P_i^{\max}\right] \ge 1 - \epsilon_{\mathtt{p}}, \tag{14}$$

$$\inf_{\mathbb{P}\in\Omega_{\mathtt{p},t}} \mathbb{P}\left[0 \le p_{i,t}^{\mathtt{c}}(\boldsymbol{e}) + r_{i,t}^{\mathtt{c}} \le x_{i,t}^{\mathtt{c}} P_i^{\max}\right] \ge 1 - \epsilon_{\mathtt{p}}, \tag{15}$$

where $P_i^{\max}$ is the maximum discharging/charging power, and $\{x_{i,t}^{\mathtt{d}}, x_{i,t}^{\mathtt{c}}\}$ are binary variables satisfying

$$x_{i,t}^{\mathtt{d}}, x_{i,t}^{\mathtt{c}} \in \{0, 1\}, \quad x_{i,t}^{\mathtt{d}} + x_{i,t}^{\mathtt{c}} = 1, \tag{16}$$

which means that battery i is either discharged or charged in t. Define $\boldsymbol{x} \coloneqq \{\boldsymbol{x}_i\}_{i\in\boldsymbol{I}}$ where $\boldsymbol{x}_i \coloneqq \{x_{i,t}^{\mathtt{d}}, x_{i,t}^{\mathtt{c}}\}_{t\in\boldsymbol{T}}$. In (14) and (15), $\epsilon_{\mathtt{p}} > 0$ is the safety parameter, a small constant. A smaller $\epsilon_{\mathtt{p}}$ implies a smaller chance to violate the power bounds $[0, P_i^{\max}]$.

Similarly, from (12), we define a vector $\boldsymbol{e}_{\mathtt{s},t} \coloneqq \{e_{\mathtt{D},1}, \ldots, e_{\mathtt{D},t}, e_{\mathtt{W},1}, \ldots, e_{\mathtt{W},t}, e_{\mathtt{d}}, e_{\mathtt{c}}\}$ representing the uncertainty relating to $s_{i,t+1}(\boldsymbol{e})$, with a covariance matrix denoted as $\Sigma_{\mathtt{s},t}$. Similar to (13), define an ambiguity set $\Omega_{\mathtt{s},t}$ with respect to $\boldsymbol{e}_{\mathtt{s},t}$. The chance constraint for $s_{i,t+1}(\boldsymbol{e})$ for $i \in \boldsymbol{I}, t \in \boldsymbol{T}$ is given by

$$\inf_{\mathbb{P}\in\Omega_{\mathtt{s},t}} \mathbb{P}\left[S_i^{\min} \le s_{i,t+1}(\boldsymbol{e}) \le S_i^{\max}\right] \ge 1 - \epsilon_{\mathtt{s}}, \tag{17}$$

where $S_i^{\min}$ and $S_i^{\max}$ are the minimum and maximum energy states of battery i, respectively, and $\epsilon_{\mathtt{s}} > 0$ indicates the chance to violate the energy bounds $[S_i^{\min}, S_i^{\max}]$. Recall that the uncertainty of PFC is modeled in the time domain in the previous subsection. Thus, the power chance constraints (14) and (15) only include the uncertainty of balancing, while the energy chance constraint (17) includes the uncertainties of both balancing and PFC.

III. Problem Formulation

A. System Cost Minimization

Let $Q_t^{\mathtt{b}}$ and $Q_t^{\mathtt{s}}$ be the prices (\$/kWh) at which the system buys energy from and sells energy to the grid, respectively. The cost of trading energy with the grid in t is given by $Q_t^{\mathtt{b}} g_t^{\mathtt{b}} - Q_t^{\mathtt{s}} g_t^{\mathtt{s}}$. Let $Q_{\mathtt{m}}$ be the price (\$/kW) of providing PFC to the grid for one day. The corresponding income is $Q_{\mathtt{m}} r_{\mathtt{m}}$.

Quadratic functions [15], [20] are used to quantify the battery discharging and charging costs: $\vartheta_{n,i}(\chi) = C_{n2,i}\chi^2 + C_{n1,i}\chi, \forall n \in \{\mathtt{d}, \mathtt{c}\}$, where $\{C_{n2,i}, C_{n1,i}\}$ are constants. The system cost minimization problem is given by

$$\begin{aligned}\min_{\boldsymbol{g},\boldsymbol{p},\boldsymbol{a},\boldsymbol{r},\boldsymbol{x}} \ & \sum_{t\in\boldsymbol{T}}\left(Q_t^{\mathtt{b}} g_t^{\mathtt{b}} - Q_t^{\mathtt{s}} g_t^{\mathtt{s}}\right) - Q_{\mathtt{m}} r_{\mathtt{m}} \\ & + \sum_{\substack{n\in\{\mathtt{d},\mathtt{c}\},\\ i\in\boldsymbol{I},t\in\boldsymbol{T}}} \mathrm{E}\left[\vartheta_{n,i}\left(p_{i,t}^n(\boldsymbol{e}) + r_{i,t}^n(E_n + e_n)\right)\right], \qquad (18)\\ \text{s.t.} \ & (1),\ (2),\ (4)\text{–}(9),\ (12),\ (14)\text{–}(17),\end{aligned}$$

where a new index $n \in \{\mathtt{d}, \mathtt{c}\}$ is used to represent discharging or charging. It can be found that (3) is equivalent to (1) if (4)–(6) hold, so (3) is omitted here. It is difficult to directly solve problem (18) due to the random variables $\boldsymbol{e}$ and chance constraints (14), (15), (17). In what follows, we reformulate problem (18) to a deterministic form.

B. Problem Reformulation

1) Objective Function: To simplify the problem, we assume that the entries in $\boldsymbol{e}$ are uncorrelated with each other. This assumption is acceptable if the uncertainty in the system is mostly caused by discrete and changeable factors. For example, demand uncertainties $\{e_{\mathtt{D},t}\}_{t\in\boldsymbol{T}}$ are generally uncorrelated if they are caused by the random use of, say, elevators, motion sensor lights, and automatic doors. The uncorrelation assumption is often used in related works [2], [13], [14] for model/problem simplification. By this assumption, we have $\mathrm{Var}[e_{\mathtt{D},t} - e_{\mathtt{W},t}] = \sigma_{\mathtt{D},t}^2 + \sigma_{\mathtt{W},t}^2$ and $\mathrm{E}[e_{\mathtt{D},t}e_n] = \mathrm{E}[e_{\mathtt{W},t}e_n] = 0$ where $n \in \{\mathtt{d}, \mathtt{c}\}$. Then, the expectation in (18) can be expressed in a deterministic form:

$$\begin{aligned}&\mathrm{E}\left[\vartheta_{n,i}\left(p_{i,t}^n(\boldsymbol{e}) + r_{i,t}^n(E_n + e_n)\right)\right]\\ &= C_{n2,i}\left(p_{i,t}^n\right)^2 + C_{n2,i}\left(\sigma_{\mathtt{D},t}^2 + \sigma_{\mathtt{W},t}^2\right)\left(a_{i,t}^n\right)^2\\ &\quad + C_{n2,i}\left(E_n^2 + \sigma_n^2\right)\left(r_{i,t}^n\right)^2 + 2C_{n2,i}E_n p_{i,t}^n r_{i,t}^n\\ &\quad + C_{n1,i}p_{i,t}^n + C_{n1,i}E_n r_{i,t}^n, \qquad (19)\end{aligned}$$

which is a nonconvex function due to the bilinear term $p_{i,t}^n r_{i,t}^n$.

2) Convex Envelopes: We eliminate the bilinear terms by relaxing them to their convex envelopes, similar to [21]. A bilinear term pr with $P_{\mathtt{l}} \le p \le P_{\mathtt{u}}$ and $R_{\mathtt{l}} \le r \le R_{\mathtt{u}}$ can be relaxed to a convex envelope h defined as

$$\begin{aligned}&h \ge P_{\mathtt{l}}r + pR_{\mathtt{l}} - P_{\mathtt{l}}R_{\mathtt{l}}, \quad h \ge P_{\mathtt{u}}r + pR_{\mathtt{u}} - P_{\mathtt{u}}R_{\mathtt{u}},\\ &h \le P_{\mathtt{l}}r + pR_{\mathtt{u}} - P_{\mathtt{l}}R_{\mathtt{u}}, \quad h \le P_{\mathtt{u}}r + pR_{\mathtt{l}} - P_{\mathtt{u}}R_{\mathtt{l}},\end{aligned}$$

which is known as McCormick envelopes [22]. In our model, we have $0 \le p_{i,t}^n, r_{i,t}^n \le P_i^{\max}$. Thus, the bilinear term $p_{i,t}^n r_{i,t}^n$ can be relaxed to

$$\begin{aligned}&p_{i,t}^n r_{i,t}^n \ge 0, \quad p_{i,t}^n r_{i,t}^n \ge P_i^{\max}\left(r_{i,t}^n + p_{i,t}^n\right) - \left(P_i^{\max}\right)^2, \qquad (20a)\\ &p_{i,t}^n r_{i,t}^n \le P_i^{\max} p_{i,t}^n, \quad p_{i,t}^n r_{i,t}^n \le P_i^{\max} r_{i,t}^n, \qquad (20b)\end{aligned}$$

where we take $p_{i,t}^n r_{i,t}^n$ as a new individual variable. Define $\boldsymbol{pr} \coloneqq \{\boldsymbol{pr}_i\}_{i\in\boldsymbol{I}}$ where $\boldsymbol{pr}_i \coloneqq \{p_{i,t}^n r_{i,t}^n\}_{n\in\{\mathtt{d},\mathtt{c}\},t\in\boldsymbol{T}}$.

3) Chance Constraints: As per [15], a chance constraint in the form of

$$\inf_{\mathbb{P}\in\Omega} \mathbb{P}\left[\left|\boldsymbol{v}^\top\boldsymbol{e} + \boldsymbol{w}\right| \le U\right] \ge 1 - \epsilon \qquad (21)$$

can be exactly reformulated as a set of deterministic inequalities:

$$\begin{aligned}&y^2 + \boldsymbol{v}^\top\Sigma\boldsymbol{v} \le \epsilon(U - z)^2, \quad |\boldsymbol{w}| \le y + z,\\ &0 \le y, \quad 0 \le z \le U, \qquad (22)\end{aligned}$$

where $\{y, z\}$ are auxiliary variables; Σ denotes the covariance matrix of the random vector $\boldsymbol{e}$. In (21), Ω is the ambiguity set defined with respect to $\boldsymbol{e}$, similar to (13). Here, we first write the chance constraints (14), (15), (17) in the form of (21), and then transform them into the form of (22). Define auxiliary variables $\{\boldsymbol{y}, \boldsymbol{z}\} \coloneqq \{\boldsymbol{y}_i, \boldsymbol{z}_i\}_{i\in\boldsymbol{I}}$ where $\{\boldsymbol{y}_i, \boldsymbol{z}_i\} \coloneqq \{y_{i,t}^n, z_{i,t}^n\}_{n\in\{\mathtt{d},\mathtt{c},\mathtt{s}\},t\in\boldsymbol{T}}$. We have

$$\begin{aligned}&\left(y_{i,t}^n\right)^2 + \left(\sigma_{\mathtt{D},t}^2 + \sigma_{\mathtt{W},t}^2\right)\left(a_{i,t}^n\right)^2 \le \epsilon_{\mathtt{p}}\left(U_{i,t}^n - z_{i,t}^n\right)^2, \qquad (23a)\\ &\left|p_{i,t}^n - U_{i,t}^n\right| \le y_{i,t}^n + z_{i,t}^n, \qquad (23b)\\ &0 \le y_{i,t}^n, \quad 0 \le z_{i,t}^n \le U_{i,t}^n \coloneqq \left(x_{i,t}^n P_i^{\max} - r_{i,t}^n\right)/2, \qquad (23c)\end{aligned}$$

where $n \in \{\mathtt{d}, \mathtt{c}\}$ corresponding to (14) and (15), respectively. We have

$$\begin{aligned}&\left(y_{i,t}^{\mathtt{s}}\right)^2 + M_{i,t}^{\mathtt{s}} \le \epsilon_{\mathtt{s}}\left[\left(S_i^{\max} - S_i^{\min}\right)/2 - z_{i,t}^{\mathtt{s}}\right]^2, \qquad (24a)\\ &\left|\Lambda_{i,t}^{\mathtt{s}}\right| \le y_{i,t}^{\mathtt{s}} + z_{i,t}^{\mathtt{s}}, \qquad (24b)\\ &0 \le y_{i,t}^{\mathtt{s}}, \quad 0 \le z_{i,t}^{\mathtt{s}} \le \left(S_i^{\max} - S_i^{\min}\right)/2, \qquad (24c)\\ &M_{i,t}^{\mathtt{s}} \coloneqq \sum_{\tau=1}^{t}\left(\sigma_{\mathtt{D},\tau}^2 + \sigma_{\mathtt{W},\tau}^2\right)\left(\eta_i^{\mathtt{c}} a_{i,\tau}^{\mathtt{c}} + \frac{1}{\eta_i^{\mathtt{d}}} a_{i,\tau}^{\mathtt{d}}\right)^2\\ &\qquad + \sigma_{\mathtt{c}}^2\left(\eta_i^{\mathtt{c}}\sum_{\tau=1}^{t} r_{i,\tau}^{\mathtt{c}}\right)^2 + \sigma_{\mathtt{d}}^2\left(\frac{1}{\eta_i^{\mathtt{d}}}\sum_{\tau=1}^{t} r_{i,\tau}^{\mathtt{d}}\right)^2, \qquad (24d)\\ &\Lambda_{i,t}^{\mathtt{s}} \coloneqq \sum_{\tau=1}^{t}\left[\eta_i^{\mathtt{c}}\left(p_{i,\tau}^{\mathtt{c}} + E_{\mathtt{c}} r_{i,\tau}^{\mathtt{c}}\right) - \frac{1}{\eta_i^{\mathtt{d}}}\left(p_{i,\tau}^{\mathtt{d}} + E_{\mathtt{d}} r_{i,\tau}^{\mathtt{d}}\right)\right]\\ &\qquad + s_{i,1} - \left(S_i^{\max} + S_i^{\min}\right)/2, \qquad (24e)\end{aligned}$$

corresponding to (17). Note that (23a) and (24a) are second-order cone (SOC) constraints because of the uncorrelation assumption.

C. Mixed-Integer Second-Order Cone Program (MISOCP)

By taking $p_{i,t}^n r_{i,t}^n$ as an individual variable, we write the battery cost function (19) as $\varphi_{i,t}^n(p_{i,t}^n, a_{i,t}^n, r_{i,t}^n, p_{i,t}^n r_{i,t}^n)$. Problem (18) can be transformed to the following MISOCP:

$$\begin{aligned}\min_{\substack{\boldsymbol{g},\boldsymbol{p},\boldsymbol{a},\boldsymbol{r},\boldsymbol{x},\\ \boldsymbol{y},\boldsymbol{z},\boldsymbol{pr}}} \ & \sum_{t\in\boldsymbol{T}}\left(Q_t^{\mathtt{b}} g_t^{\mathtt{b}} - Q_t^{\mathtt{s}} g_t^{\mathtt{s}}\right) - Q_{\mathtt{m}} r_{\mathtt{m}}\\ & + \sum_{\substack{n\in\{\mathtt{d},\mathtt{c}\},\\ i\in\boldsymbol{I},t\in\boldsymbol{T}}} \varphi_{i,t}^n(p_{i,t}^n, a_{i,t}^n, r_{i,t}^n, p_{i,t}^n r_{i,t}^n), \qquad (25)\\ \text{s.t.} \ & (1),\ (2),\ (6)\text{–}(9),\ (16),\ (20),\ (23),\ (24).\end{aligned}$$

This problem is a relaxation of problem (18) due to (20), but the impact of the relaxation on the optimal objective value would be small since E_n is generally small in practice ($E_n \approx 0.066$ h in simulation). Note that the relaxation

only applies to the objective function, so any feasible solution to problem (25) is still feasible to the original problem (18). Constraints $g_t^{\mathrm{b}} g_t^{\mathrm{s}} = 0$ and $a_{i,t}^{\mathrm{d}} a_{i,t}^{\mathrm{c}} = 0$ are not included in problem (25) as they can be satisfied automatically (see Appendix A).

MISOCP is mostly NP-hard and can be solved by exact algorithms (e.g., branch and bound) via off-the-shelf solvers (e.g., CPLEX). See [23] for a review of the algorithms and solvers for convex mixed-integer nonlinear programs (MINLP). However, if the time spent by exact algorithms to get the optimal solution is too long, we may resort to heuristics. For instance, we set up problem (25) with 3 batteries and 24 time periods, and CPLEX was unable to prove the optimality of the solution in 10 hours. For practicality, a heuristic is developed in the next section to get suboptimal solutions quickly.

IV. Solution

A. Penalty Alternating Direction Method (PADM)

Based on PADM [16], we develop a heuristic to obtain a suboptimal solution to problem (25) quickly. First, we transform problem (25) to make it suitable for the PADM framework. Let the objective of problem (25) be written as $\min_{\boldsymbol{Y}} f(\boldsymbol{Y})$, and let $\boldsymbol{Y} \in \mathcal{Y}$ denote the continuous relaxation of the constraints in (25), i.e., $x_{i,t}^n \in \{0,1\}$ is relaxed to $0 \le x_{i,t}^n \le 1$. Define auxiliary variables $\boldsymbol{Z} := \{Z_{i,t}^n\}_{n\in\{\mathrm{d},\mathrm{c}\},i\in\boldsymbol{I},t\in\boldsymbol{T}}$ and an integer set $\mathcal{Z} := \{\boldsymbol{Z} \mid Z_{i,t}^n \in \{0,1\}, Z_{i,t}^{\mathrm{d}} + Z_{i,t}^{\mathrm{c}} = 1\}$. Problem (25) can be written in an equivalent form:

$$\min_{\boldsymbol{Y},\boldsymbol{Z}} f(\boldsymbol{Y}), \quad \text{s.t. } \boldsymbol{Y} \in \mathcal{Y},\ \boldsymbol{Z} \in \mathcal{Z},\ \boldsymbol{x} = \boldsymbol{Z},$$

where $\boldsymbol{x}$ is part of $\boldsymbol{Y}$. By the definitions of $\boldsymbol{x}$ and $\boldsymbol{Z}$, we have $|x_{i,t}^{\mathrm{d}} - Z_{i,t}^{\mathrm{d}}| = |x_{i,t}^{\mathrm{c}} - Z_{i,t}^{\mathrm{c}}|$. This implies that we can simplify the constraint $\boldsymbol{x} = \boldsymbol{Z}$ to either $x_{i,t}^{\mathrm{d}} = Z_{i,t}^{\mathrm{d}}$ or $x_{i,t}^{\mathrm{c}} = Z_{i,t}^{\mathrm{c}}$. Here we choose the former, which is further decomposed into

$$x_{i,t}^{\mathrm{d}} \ge Z_{i,t}^{\mathrm{d}}, \quad x_{i,t}^{\mathrm{d}} \le Z_{i,t}^{\mathrm{d}}.$$

Then, we penalize them in the objective function. The resulting penalty problem is given by

$$\begin{aligned} \min_{\boldsymbol{Y},\boldsymbol{Z}} \ & \alpha W f(\boldsymbol{Y}) + (1-\alpha) \sum_{i\in\boldsymbol{I},t\in\boldsymbol{T}} \Big(\rho_{i,t}^0 \big[x_{i,t}^{\mathrm{d}} - Z_{i,t}^{\mathrm{d}}\big]^+ \\ & \qquad + \rho_{i,t}^1 \big[Z_{i,t}^{\mathrm{d}} - x_{i,t}^{\mathrm{d}}\big]^+ \Big), \quad (26) \\ \text{s.t.} \ & \boldsymbol{Y} \in \mathcal{Y}, \quad \boldsymbol{Z} \in \mathcal{Z}, \end{aligned}$$

where $[\chi]^+$ means $\max\{0,\chi\}$; $\boldsymbol{\rho} := \{\rho_{i,t}^0, \rho_{i,t}^1\}_{i\in\boldsymbol{I},t\in\boldsymbol{T}}$ are penalty parameters; $0 \le \alpha \le 1$ is a weight parameter for balancing the system cost f and penalty; W is a normalization factor [16].

Next, we employ PADM to solve problem (26), as shown in Algorithm 1. The objective function in (26) is written as $\phi(\boldsymbol{Y},\boldsymbol{Z};\boldsymbol{\rho},\alpha)$. The algorithm is composed of two loops. The inner loop, indexed by m, is a standard ADM that can converge to *partial minima* of problem (26) when $\{\boldsymbol{\rho},\alpha\}$ are given [16]. The two problems (27) and (28) can be simplified as follows.

Algorithm 1: Heuristic Based on PADM

Input: $m = 0$, $\{\boldsymbol{Y}^0, \boldsymbol{Z}^0\}$, $\boldsymbol{\rho} > \boldsymbol{0}$, $\Delta\rho > 0$, $\alpha = 1$, $0 < \theta < 1$.
Output: Integer solution $\boldsymbol{Z}^*$
Normalization factor: $W = \sqrt{TI}\|\nabla f(\boldsymbol{Y}^0)\|_2^{-1}$.
repeat // Outer loop
  repeat // Inner loop
    Continuous solution: $\boldsymbol{Y}^{m+1}$

$$= \arg\min_{\boldsymbol{Y}} \{\phi(\boldsymbol{Y}, \boldsymbol{Z}^m; \boldsymbol{\rho}, \alpha) \mid \boldsymbol{Y} \in \mathcal{Y}\}. \quad (27)$$

    Integer solution: $\boldsymbol{Z}^{m+1}$

$$= \arg\min_{\boldsymbol{Z}} \{\phi(\boldsymbol{Y}^{m+1}, \boldsymbol{Z}; \boldsymbol{\rho}, \alpha) \mid \boldsymbol{Z} \in \mathcal{Z}\}. \quad (28)$$

    Inner loop index: $m \leftarrow m + 1$.
  until $\boldsymbol{Z}^m = \boldsymbol{Z}^{m-1}$;
  Weight parameter update: $\alpha \leftarrow \theta\alpha$.
  Penalty parameter update:

$$\rho_{i,t}^0 \leftarrow \rho_{i,t}^0 + \Delta\rho, \quad \text{if } Z_{i,t}^{\mathrm{d},m} = 0. \quad (29)$$

$$\rho_{i,t}^1 \leftarrow \rho_{i,t}^1 + \Delta\rho, \quad \text{if } Z_{i,t}^{\mathrm{d},m} = 1. \quad (30)$$

until $\boldsymbol{x}^m = \boldsymbol{Z}^m$;

Due to $Z_{i,t}^{\mathrm{d},m} \in \{0,1\}$, the objective in (27) can be written as

$$\begin{aligned} \min_{\boldsymbol{Y}} \ & \alpha W f(\boldsymbol{Y}) + (1-\alpha) \sum_{\{i,t\}:Z_{i,t}^{\mathrm{d},m}=0} \rho_{i,t}^0 x_{i,t}^{\mathrm{d}} \\ & + (1-\alpha) \sum_{\{i,t\}:Z_{i,t}^{\mathrm{d},m}=1} \rho_{i,t}^1 \big(1 - x_{i,t}^{\mathrm{d}}\big). \quad (31) \end{aligned}$$

This shows that problem (27) is a convex program. In problem (28), $f(\boldsymbol{Y}^{m+1})$ is a constant, so the solution $\boldsymbol{Z}^{m+1}$ can be directly given by

$$Z_{i,t}^{\mathrm{d},m+1} = \begin{cases} 0, & \text{if } \rho_{i,t}^0 x_{i,t}^{\mathrm{d},m+1} \le \rho_{i,t}^1 \Big(1 - x_{i,t}^{\mathrm{d},m+1}\Big); \\ 1, & \text{otherwise.} \end{cases} \quad (32)$$

In the outer loop, weight parameter α and penalty parameters $\boldsymbol{\rho}$ are updated. The purpose of updating α is to obtain a feasible solution. α will gradually decrease to increasingly emphasize the penalty terms so as to reach $\boldsymbol{x} = \boldsymbol{Z}$. The purpose of updating $\boldsymbol{\rho}$ is to obtain a good integer solution $\boldsymbol{Z}$. The idea is to use perturbation that allows the algorithm to try different choices of integers. Here, the perturbation is implemented by the penalty parameter update in (29) and (30). Fig. 2 shows the effect of (29) and (30) on integer solution $Z_{i,t}^{\mathrm{d}}$ if $x_{i,t}^{\mathrm{d}}$ is fixed. It can be seen that if $x_{i,t}^{\mathrm{d}}$ is far from both 0 and 1 ($x_{i,t}^{\mathrm{d}} = 0.5, 0.7$), then $Z_{i,t}^{\mathrm{d}}$ is frequently shifted between 0 and 1. This can be understood as strong perturbation that lets the algorithm keep trying between $Z_{i,t}^{\mathrm{d}} = 0$ and $Z_{i,t}^{\mathrm{d}} = 1$. Fig. 2 also shows that if $x_{i,t}^{\mathrm{d}}$ is closer to 0 or 1, then less perturbation appears. This can assist the algorithm in converging to $x_{i,t}^{\mathrm{d}} \approx Z_{i,t}^{\mathrm{d}}$. Fig. 2 is only used for demonstrating the effect of the penalty parameter update. In fact, $x_{i,t}^{\mathrm{d}}$ is given by the solution to problem (27), so $x_{i,t}^{\mathrm{d}}$ is generally varying (not fixed) in the algorithm. Therefore, the perturbation frequency can adapt to $x_{i,t}^{\mathrm{d}}$, helping the inner loop reach $x_{i,t}^{\mathrm{d}} \approx Z_{i,t}^{\mathrm{d}}$.

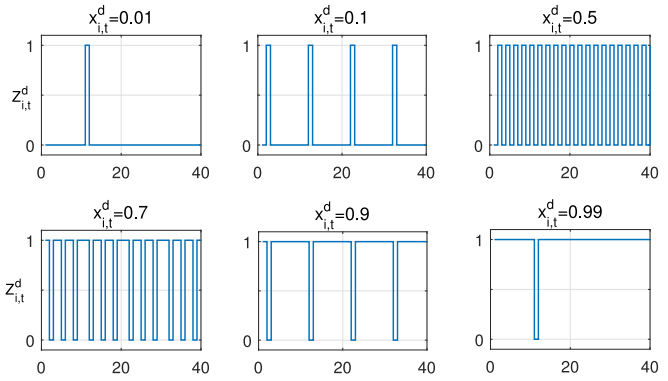

Fig. 2. The effect of the penalty parameter update on integer solution $Z^{\mathrm{d}}_{i,t}$ in the case that $x^{\mathrm{d}}_{i,t}$ is fixed and $\Delta\rho = 10$. The x-axes denote the iteration of the outer loop in Algorithm 1.

In summary, the inner loop of Algorithm 1 is responsible for providing a partial minimum of penalty problem (26) with given $\boldsymbol{\rho}$ and α. Note that the partial minima satisfy $\boldsymbol{Y} \in \mathcal{Y}$ and $\boldsymbol{Z} \in \mathcal{Z}$. In the outer loop, the update of $\boldsymbol{\rho}$ helps the inner loop explore different integer solutions and converge to $\boldsymbol{x} \approx \boldsymbol{Z}$. The update of α gradually emphasizes the penalty terms in (26) for reaching $\boldsymbol{x} = \boldsymbol{Z}$. Therefore, if Algorithm 1 terminates, it can return a feasible solution to the original problem (25).

B. Implementation

According to (8), if the system provides PFC ($r_{\mathrm{m}} > 0$), it should ensure both $\sum_{i\in\boldsymbol{I}} r^{\mathrm{d}}_{i,t} > 0$ and $\sum_{i\in\boldsymbol{I}} r^{\mathrm{c}}_{i,t} > 0$ for every $t \in \boldsymbol{T}$. This means that the system needs at least one battery with $x^{\mathrm{d}}_{i,t} = 1$ and at least one battery with $x^{\mathrm{c}}_{j,t} = 1, j \neq i$ for every t. But, the integer solution given by (32) often yields $\sum_{i\in\boldsymbol{I}} Z^{\mathrm{d}}_{i,t} = 0$ or $\sum_{i\in\boldsymbol{I}} Z^{\mathrm{d}}_{i,t} = I$ for some t, which results in $r_{\mathrm{m}} = 0$, i.e., no PFC service. To guarantee the availability of PFC, we can add the following constraint to problem (28).

$$1 \leq \sum_{i\in\boldsymbol{I}} Z^{\mathrm{d}}_{i,t} \leq I - 1. \tag{33}$$

When Algorithm 1 starts, $\boldsymbol{Y}^0$ can be given by the solution to $\{\min_{\boldsymbol{Y}} f(\boldsymbol{Y}) \mid \boldsymbol{Y} \in \mathcal{Y}\}$, while $\boldsymbol{Z}^0$ can be randomly generated (because of the initial value of $\alpha = 1$). For implementation, we change the outer loop stopping condition to $\|\boldsymbol{x}^m - \boldsymbol{Z}^m\|_\infty < 10^{-3}$ and $\|\boldsymbol{x}^m - \boldsymbol{x}^{m-1}\|_\infty < 10^{-5}$, where the second inequality ensures the stability of the results. When Algorithm 1 terminates, we only use the resulting integer solution $\boldsymbol{Z}^*$. Then, we solve the MISOCP (25) with $\boldsymbol{x} = \boldsymbol{Z}^*$ to get the final continuous solution $\boldsymbol{Y}^*$.

V. Pricing for Multiple Services

A. Local Market

Similar to [20], we employ duality to determine the prices of the services. By fixing binary variables to $\boldsymbol{x} = \boldsymbol{Z}^*$, the MISOCP (25) becomes a SOCP. Hereafter, *the SOCP* refers to the MISOCP (25) with $\boldsymbol{x} = \boldsymbol{Z}^*$. Due to the convexity of the SOCP, we define the service prices as follows.

1) For load shifting, define λ_t as the multiplier of energy balance constraint (1). It is the energy price (\$/kWh) at which the batteries and load trade energy in the system at t. Define $\boldsymbol{\lambda} := \{\lambda_t\}_{t\in\boldsymbol{T}}$.
2) For balancing, define μ_t as the multiplier of constraint (6). It is the payment (\$) made by the load for buying balancing reserve in t. Define $\boldsymbol{\mu} := \{\mu_t\}_{t\in\boldsymbol{T}}$.
3) For PFC, define π^{d}_t and π^{c}_t as the multipliers of the two constraints in (8), respectively. They are the prices (\$/kW) of discharging and charging power reserved for PFC in t. Define $\boldsymbol{\pi} := \{\pi^{\mathrm{d}}_t, \pi^{\mathrm{c}}_t\}_{t\in\boldsymbol{T}}$.

With the prices $\boldsymbol{\Phi} := \{\boldsymbol{\lambda}, \boldsymbol{\mu}, \boldsymbol{\pi}\}$, we analyze the system from a market perspective. Here, we consider a local market with two types of agents: batteries and a system manager. For battery $i \in \boldsymbol{I}$, its individual utility maximization problem is given by

$$\begin{aligned}\max_{\substack{\boldsymbol{p}_i,\boldsymbol{a}_i,\boldsymbol{r}_i,\\ \boldsymbol{y}_i,\boldsymbol{z}_i,\boldsymbol{pr}_i}} \ & \sum_{t\in\boldsymbol{T}}\left[\lambda_t\left(p^{\mathrm{d}}_{i,t} - p^{\mathrm{c}}_{i,t}\right) + \mu_t\left(a^{\mathrm{d}}_{i,t} + a^{\mathrm{c}}_{i,t}\right) + \pi^{\mathrm{d}}_t r^{\mathrm{d}}_{i,t} + \pi^{\mathrm{c}}_t r^{\mathrm{c}}_{i,t}\right] \\ & - \sum_{\substack{t\in\boldsymbol{T},\\ n\in\{\mathrm{d},\mathrm{c}\}}} \varphi^n_{i,t}(p^n_{i,t}, a^n_{i,t}, r^n_{i,t}, p^n_{i,t}r^n_{i,t}), \qquad (34)\\ \text{s.t.} \ & p^n_{i,t} \geq 0, a^n_{i,t} \geq 0, \quad r^n_{i,t} \geq 0, \forall n \in \{\mathrm{d},\mathrm{c}\}, t \in \boldsymbol{T}, \\ & \text{Relaxation constraints: (20)}, \forall n \in \{\mathrm{d},\mathrm{c}\}, t \in \boldsymbol{T}, \\ & \text{Power constraints: (23)}, \forall n \in \{\mathrm{d},\mathrm{c}\}, t \in \boldsymbol{T}, \\ & \text{Energy constraints: (24)}, \forall t \in \boldsymbol{T}.\end{aligned}$$

In this problem, $\boldsymbol{x}$ is fixed to $\boldsymbol{Z}^*$. As shown by the objective function (34), a battery's utility is defined as the incomes minus the operating cost. The system manager is a non-profit agent, acting as an interface between the grid and batteries. The system manager's problem is given by

$$\begin{aligned}\max_{\boldsymbol{g},r_{\mathrm{m}}} \ & Q_{\mathrm{m}} r_{\mathrm{m}} - \sum_{i\in\boldsymbol{I}}\sum_{t\in\boldsymbol{T}}\left(\pi^{\mathrm{d}}_t r^{\mathrm{d}}_{i,t} + \pi^{\mathrm{c}}_t r^{\mathrm{c}}_{i,t}\right) \\ & + \sum_{t\in\boldsymbol{T}}\left(Q^{\mathrm{s}}_t g^{\mathrm{s}}_t - Q^{\mathrm{b}}_t g^{\mathrm{b}}_t\right) \\ & + \sum_{t\in\boldsymbol{T}} \lambda_t \left[\sum_{i\in\boldsymbol{I}}\left(p^{\mathrm{c}}_{i,t} - p^{\mathrm{d}}_{i,t}\right) + D_t - W_t\right], \qquad (35)\\ \text{s.t.} \ & r_{\mathrm{m}} \geq 0, \quad g^{\mathrm{b}}_t \geq 0, \quad g^{\mathrm{s}}_t \geq 0, \forall t \in \boldsymbol{T}.\end{aligned}$$

The objective (35) is defined as the PFC payment from the grid minus the PFC payments to batteries plus the energy payments from the grid, batteries, and load. *The market clearing conditions* are

$$[\lambda_t]: \ \sum_{i\in\boldsymbol{I}}\left(p^{\mathrm{d}}_{i,t} - p^{\mathrm{c}}_{i,t}\right) + g^{\mathrm{b}}_t - g^{\mathrm{s}}_t = D_t - W_t, \forall t \in \boldsymbol{T}, \tag{36a}$$

$$[\mu_t]: \ \sum_{i\in\boldsymbol{I}}\left(a^{\mathrm{d}}_{i,t} + a^{\mathrm{c}}_{i,t}\right) = 1, \forall t \in \boldsymbol{T}, \tag{36b}$$

$$\left[\pi^n_t\right]: \ \sum_{i\in\boldsymbol{I}} r^n_{i,t} = r_{\mathrm{m}}, \forall n \in \{\mathrm{d},\mathrm{c}\}, t \in \boldsymbol{T}, \tag{36c}$$

where $[\,\cdot\,]$ represents the multipliers, namely prices.

B. Market Properties

Here, we theoretically analyze the local market. Given the prices $\boldsymbol{\Phi}$, both the individual battery problem (34) and the manager problem (35) are convex programs, for which Karush–Kuhn–Tucker (KKT) conditions are necessary and

sufficient for optimality. Thus, the conditions (36) and the KKT conditions of problems (34) and (35) determine the market equilibrium. Proposition 1 shows the relation between the equilibrium and the SOCP.

Proposition 1 (Market Equilibrium): The scheduling result $\boldsymbol{\Theta}^* := \{\boldsymbol{g}^*, \boldsymbol{p}^*, \boldsymbol{a}^*, \boldsymbol{r}^*\}$ (given by the optimal solution to the SOCP) and the pricing result $\boldsymbol{\Phi}^* := \{\boldsymbol{\lambda}^*, \boldsymbol{\mu}^*, \boldsymbol{\pi}^*\}$ (given by the optimal multipliers of the SOCP) constitute a market equilibrium that satisfies the following properties.

1) Given the prices $\boldsymbol{\Phi}^*$, the schedule $\boldsymbol{\Theta}^*$ provides the optimal solutions to the individual battery problem (34) and the system manager problem (35).
2) The schedule $\boldsymbol{\Theta}^*$ satisfies the market clearing conditions (36).

It is obvious that $\{\boldsymbol{\Theta}^*, \boldsymbol{\Phi}^*\}$ corresponds to a point satisfying the KKT conditions of the SOCP. One can find that $\{\boldsymbol{\Theta}^*, \boldsymbol{\Phi}^*\}$ also satisfies the KKT conditions of problems (34) and (35). Thus, $\boldsymbol{\Theta}^*$ provides the optimal solutions to the two problems. The detailed proof of Proposition 1 is given in Appendix B.

In addition, the local market holds two properties: individual rationality and balanced budget, which are described in the following two propositions. The proofs are presented in Appendix.

Proposition 2 (Individual Rationality): The utility of battery i, the objective function in (34), is always non-negative in the market.

Proposition 3 (Balanced Budget): For each service, the payment made is equal to the payment received in the market (i.e., no budget deficit or surplus).

1) For load shifting, the payment made by the load is equal to the payments received by the grid and batteries:

$$\lambda_t^*(D_t - W_t) = Q_t^{\mathrm{b}} g_t^{\mathrm{b}*} - Q_t^{\mathrm{s}} g_t^{\mathrm{s}*} + \sum_{i\in\boldsymbol{I}} \lambda_t^* \left(p_{i,t}^{\mathrm{d}*} - p_{i,t}^{\mathrm{c}*}\right), \forall t \in \boldsymbol{T}. \quad (37)$$

2) For balancing, the payment made by the load is equal to the total payment received by the batteries:

$$\mu_t^* = \sum_{i\in\boldsymbol{I}} \mu_t^* \left(a_{i,t}^{\mathrm{d}*} + a_{i,t}^{\mathrm{c}*}\right), \forall t \in \boldsymbol{T}. \quad (38)$$

3) For PFC, the payment made by the grid is equal to the total payment received by the batteries:

$$Q_{\mathrm{m}} r_{\mathrm{m}}^* = \sum_{i\in\boldsymbol{I}} \sum_{t\in\boldsymbol{T}} \left(\pi_t^{\mathrm{d}*} r_{i,t}^{\mathrm{d}*} + \pi_t^{\mathrm{c}*} r_{i,t}^{\mathrm{c}*}\right). \quad (39)$$

Equations (37) and (39) imply that the manager objective function in (35) is equal to zero at the equilibrium.

VI. Numerical Results

A. Parameter Setting

Set up a system with $I = 3$ batteries (denoted as B1, B2, and B3) and a scheduling horizon of $T = 24$ hours. Load parameters $(D_t - W_t)$ (see Appendix E) are obtained by scaling the hourly consumption and wind generation forecast data from the French grid [19]. Set $\sigma_{\mathrm{D},t} = 0.2D_t$ and $\sigma_{\mathrm{W},t} = 0.2W_t$ [20]. Based on the French electricity tariffs [24], grid energy buy prices are set to $Q_t^{\mathrm{b}} = 17.98$ €cent/kWh for peak hours $t \in \{8, \ldots, 22\}$ and $Q_t^{\mathrm{b}} = 13.44$ €cent/kWh for off-peak hours $t \in \{1, \ldots, 7, 23, 24\}$. Set $Q_t^{\mathrm{s}} = 0.6Q_t^{\mathrm{b}}$. The PFC price is set to $Q_{\mathrm{m}} = 17.32$ €cent/kW that is the average price of frequency containment reserve in Dec. 2019 in France [25]. By analyzing the French frequency deviation data in Dec. 2019 [19] and selecting $f_{\mathrm{db}} = 10$ mHz and $f_{\max} = 100$ mHz (see Fig. 1), we get sampling values $E_{\mathrm{d}} = 0.0661$ h, $E_{\mathrm{c}} = 0.0669$ h, $\sigma_{\mathrm{d}} = 0.0524$ h, and $\sigma_{\mathrm{c}} = 0.0452$ h. The parameters of battery $i \in \{1, 2, 3\}$ are set as follows: $C_{n2,i} = 0.02$ €cent/kWh^2, $C_{n1,i} = 1$ €cent/kWh, $\eta_i^{\mathrm{d}} = \eta_i^{\mathrm{c}} = 0.9$, $P_i^{\max} = 1$ MW, $\{S_1^{\mathrm{B}}, S_2^{\mathrm{B}}, S_3^{\mathrm{B}}\} = \{4, 6, 8\}$ MWh, $S_i^{\max} = 0.9S_i^{\mathrm{B}}$, $S_i^{\min} = 0.1S_i^{\mathrm{B}}$, $s_{1,i} = 0.25S_i^{\mathrm{B}}$, and $\epsilon_{\mathrm{p}} = \epsilon_{\mathrm{s}} = 0.5$. Here, the batteries only differ in the capacity parameters, so we can see how capacity impacts the results.

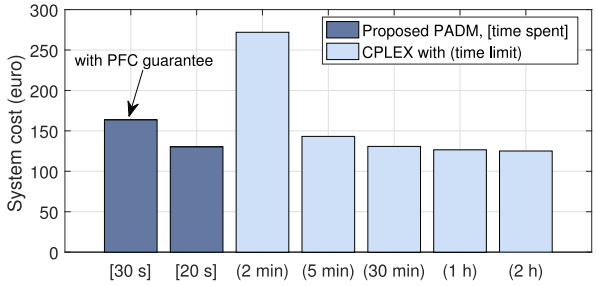

Fig. 3. System costs under the proposed PADM-based heuristic (Algorithm 1) and CPLEX (exact algorithm). PFC guarantee: constraint (33) is included in Algorithm 1.

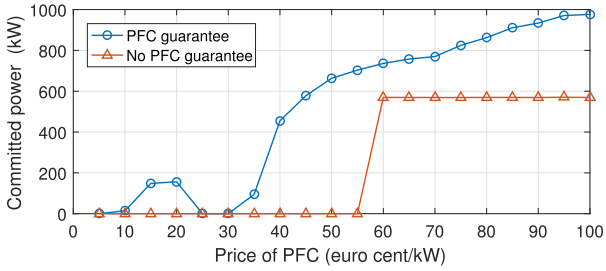

Fig. 4. The committed power r_{m} returned by Algorithm 1 versus the PFC price Q_{m}. PFC guarantee: constraint (33) is included in Algorithm 1.

B. Computational Results

For the proposed PADM-based heuristic (Algorithm 1), we initialize $\rho_{i,t}^0 = \rho_{i,t}^1 = 1$ and set $\Delta\rho = 10$, $\theta = 0.95$. As shown in Fig. 3, the time spent by the proposed heuristic to solve the MISOCP (25) is short. The resulting system cost and time spent increase after the PFC guarantee constraint (33) is included. The MISOCP (25) can be exactly solved by CPLEX, but it is greatly time-consuming due to the big problem size. For comparison, we test CPLEX with time limits and no PFC guarantee. It can be seen in Fig. 3 that the proposed solution, [20 s] €130.35, is quite comparable to the CPLEX solutions, (30 min) €130.78, (1 h) €126.54, (2 h) €125.10, showing that the proposed heuristic can return high-quality solutions quickly.

Note that apart from the [30 s] solution, all other solutions in Fig. 3 have zero PFC committed power, namely

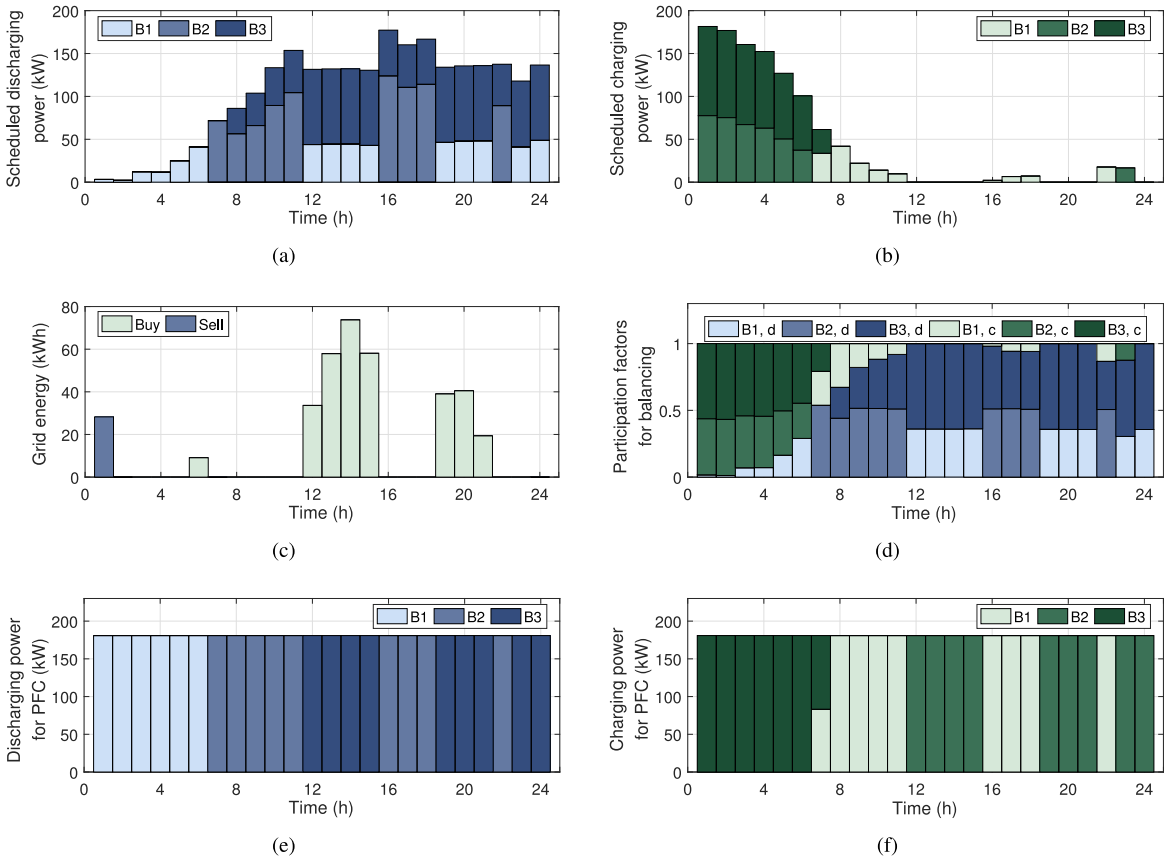

Fig. 5. Scheduling results. (a) Scheduled discharging power of batteries for load shifting, $p^{\mathrm{d}}_{i,t}$. (b) Scheduled charging power of batteries for load shifting, $p^{\mathrm{c}}_{i,t}$. (c) Energy traded with the grid, $\{g^{\mathrm{b}}_t, g^{\mathrm{s}}_t\}$. (d) Participation factors of batteries for real-time balancing, $\{a^{\mathrm{d}}_{i,t}, a^{\mathrm{c}}_{i,t}\}$. (e) Discharging power committed by batteries for PFC, $r^{\mathrm{d}}_{i,t}$. (f) Charging power committed by batteries for PFC, $r^{\mathrm{c}}_{i,t}$.

$r^*_{\mathrm{m}} = 0$. This means that providing PFC service may not be a good cost-minimizing choice under our parameter setting. One of the main reasons may be the relatively low PFC price Q_{m}. To further examine the impact of Q_{m}, we increase Q_{m} and show the solutions returned by Algorithm 1 in Fig. 4. It is shown that the relation between Q_{m} and r_{m} is not significant when Q_{m} is relatively low. If Q_{m} is high enough, the benefit from PFC will attract the system to increase the committed power. In Fig. 4, the system has a positive committed power under $Q_{\mathrm{m}} \geq 60$ €cent/kW even if the PFC guarantee constraint (33) is not included in Algorithm 1.

C. Scheduling Results

Fig. 5 shows the scheduling results under the [30 s] solution in Fig. 3. From Fig. 5(a) and Fig. 5(b), one can see that B2 and B3 are mostly discharged in peak hours and charged in off-peak hours. This is an economical decision since the system can buy less amount of expensive peak-hour energy from the grid. But, B1 acts a bit differently, discharging in off-peak hours. This results from the PFC guarantee constraint (33) that ensures at least one discharging battery and one charging battery at each hour. B2 and B3 have higher capacities than B1, i.e., B2 and B3 can store more energy. This is the reason why B2 and B3 (rather than B1) are mostly charged in off-peak hours. On the operating day, the scheduled discharging/charging power will be adjusted to respond to the realization of uncertainty. Thus, the pattern of participation factors in Fig. 5(d) is consistent with the pattern composed of Fig. 5(a) and Fig. 5(b). For PFC, it can be found from Fig. 5(e) and Fig. 5(f) that the PFC committed power, ± 180.82 kW, is collectively provided by B1, B2, and B3, satisfying constraints (8).

Fig. 6 shows how the safety parameters $\{\epsilon_{\mathrm{p}}, \epsilon_{\mathrm{s}}\}$ impact the scheduling results of B1 under uncertainty realization. In Fig. 6, the integer solution is fixed and provided by the [30 s] solution. Each subfigure in Fig. 6 contains 1000 realizations of the system uncertainty vector $\boldsymbol{e}$, in which each entry is assumed to follow a normal distribution. The power curves in Fig. 6(a) and Fig. 6(b) are given by $p^n_{i,t}(\boldsymbol{e}) + r^n_{i,t}$, and the energy curves in Fig. 6(c) and Fig. 6(d) are given by $s_{i,t+1}(\boldsymbol{e})$ in (12). It is shown that a smaller safety parameter leads to a smaller chance to violate the power/energy bounds. Also, a smaller safety parameter means a more conservative solution, leading to a higher system cost, as shown in Fig. 7. One can adjust the safety parameters to strike a balance between the system cost and power/energy bound violation. In real situations, batteries are not the only type of resources responding to uncertainty realization. Practical systems would have other resources such as local generators

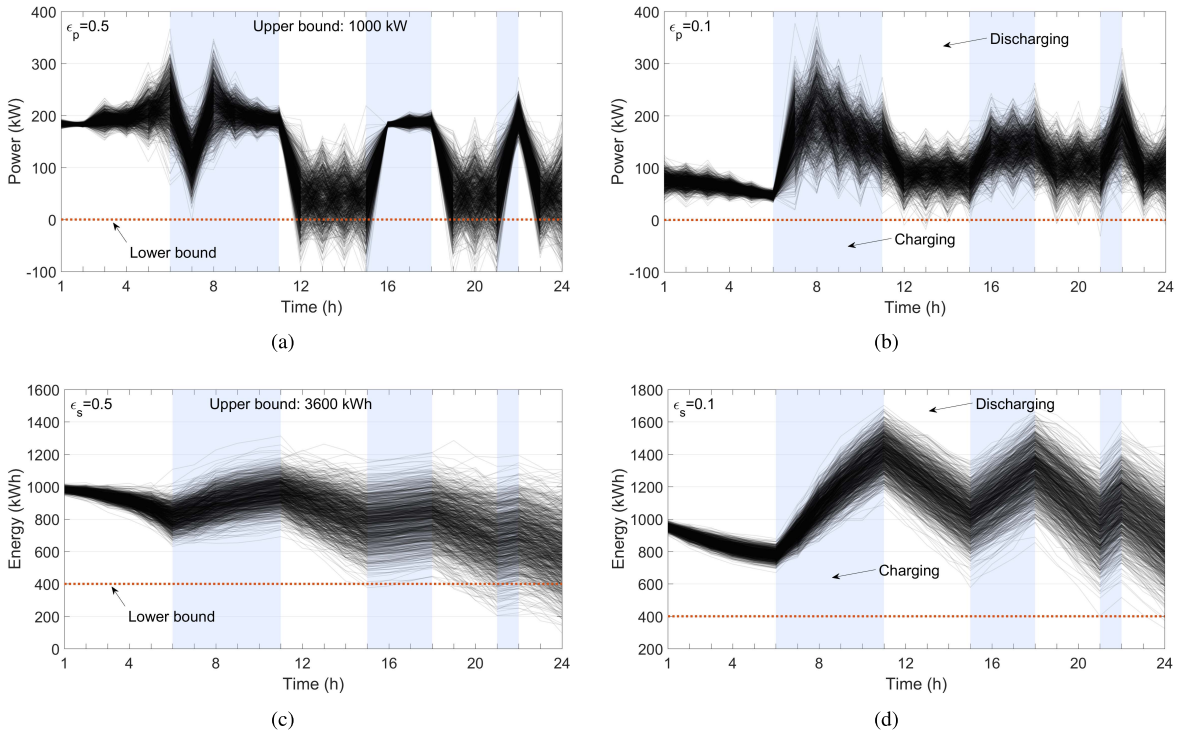

Fig. 6. Actual power and energy state of B1 with safety parameters (a) $\epsilon_{\mathrm{p}} = 0.5$, (b) $\epsilon_{\mathrm{p}} = 0.1$, (c) $\epsilon_{\mathrm{s}} = 0.5$, and (d) $\epsilon_{\mathrm{s}} = 0.1$. Each gray curve represents a realization of uncertainty. The power bounds of B1 are given by $[0, 1000]$ kW. The energy bounds of B1 are given by $[400, 3600]$ kWh.

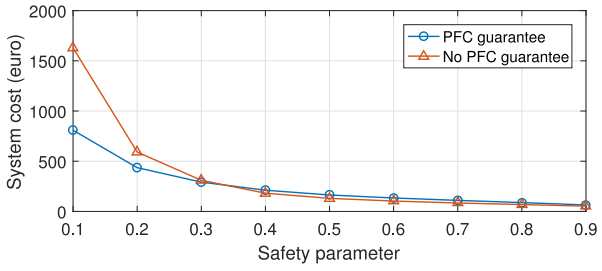

Fig. 7. System cost versus safety parameters ($\epsilon_{\mathrm{p}} = \epsilon_{\mathrm{s}}$). PFC guarantee: the integer solution is fixed and given by the [30 s] solution. No PFC guarantee: the integer solution is fixed and given by the [20 s] solution.

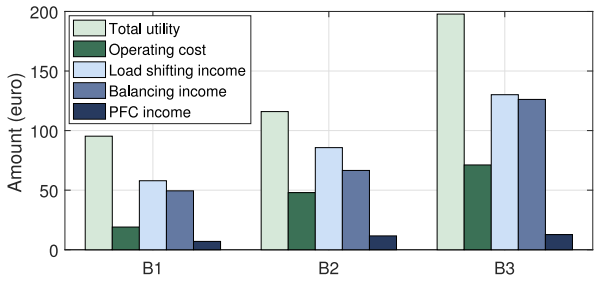

Fig. 8. Pricing results. The utility is equal to the incomes minus the cost.

and controllable loads, which can be used to compensate for the amount of battery power/energy violation on the operating day.

D. Pricing Results

Fig. 8 shows our pricing results under the [30 s] solution. It can be seen that each battery has a positive utility, which validates the property of individual rationality (Proposition 2). Also, the utilities, incomes, and costs generally go up as the battery capacity increases. For example, B3 has the highest capacity, so it can contribute more to service provisioning. As a result, it is used the most (the highest operating cost) and earns the most. The pricing results of other solutions in Fig. 3 are similar to that of the [30 s] solution. The major difference is that the other solutions have zero PFC committed power, so their PFC incomes are all zero.

To further explore the relation between battery utility and capacity, we increase the capacity of B1, S_1^{B}, and show the consequences in Fig. 9, where the energy to power ratio of B1, $S_1^{\mathrm{B}}/P_1^{\max} = 4$ h, is kept unchanged. The integer solution is fixed and given by the [30 s] solution. It can be seen that the utility of B1 grows if B1 capacity increases. The reason is that B1 can earn more by using more capacity to provide services. More capacity also leads to less system cost, as shown in Fig. 9(b). An important observation is that the rate of system cost reduction decreases as B1 capacity goes up. This is because we consider quadratic battery usage costs in (18). This is also reflected in Fig. 9(a), where the rate of B1 utility growth is slowing down, meaning that the marginal benefit of capacity is decreasing. Another observation is that the utility of B3 (8 MWh) is higher than the utility of B1 at 9 MWh in Fig. 9(a). This implies that a higher capacity does not always lead to a higher utility. But, the capacity limits how much a battery can be used. In general, under

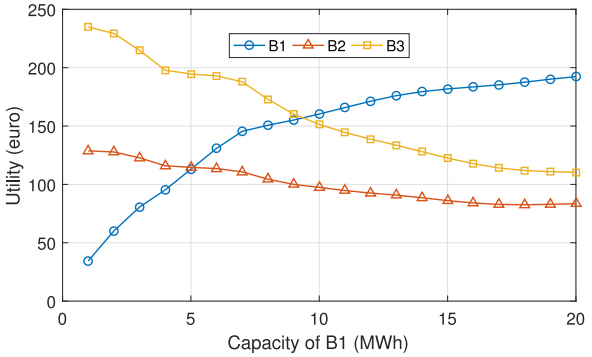

(a)

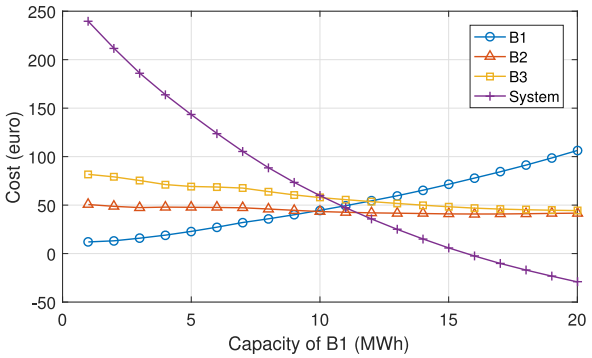

(b)

Fig. 9. Battery utilities and costs changed with B1 capacity. The capacities of B2 and B3 are fixed to 6 and 8 MWh, respectively. The cost of a battery reflects how much the battery is used.

the proposed pricing method, a battery earns more if it is used more (see B1); a battery earns less if it is used less (see B2 and B3).

VII. Conclusion

In this paper, we proposed day-ahead scheduling and pricing methods for battery energy storage to provide multiple services including load shifting, real-time balancing, and PFC. The original stochastic chance-constrained scheduling problem was reformulated to an MISOCP. To obtain suboptimal solutions quickly, we developed a PADM-based heuristic to solve the MISOCP. By fixing the integer solution returned by the heuristic, we employed the duality of the SOCP to price the three services in the local market. We also provided theoretical analysis of the market properties. Numerical results show that the proposed heuristic is computationally efficient, and the pricing results can guarantee a positive utility for each battery, i.e., service incomes are enough to cover battery usage costs.

Appendix A
Redundancy of $g_t^{\mathrm{b}} g_t^{\mathrm{s}} = 0$ and $a_{i,t}^{\mathrm{d}} a_{i,t}^{\mathrm{c}} = 0$

Suppose that there is a solution to the MISOCP (25) with $g_t^{\mathrm{b}*} > 0$ and $g_t^{\mathrm{s}*} > 0$ for a fixed t. Discuss two cases:

1) $g_t^{\mathrm{b}*} \geq g_t^{\mathrm{s}*}$. In this case, let $g_t^{\mathrm{b}\prime} = g_t^{\mathrm{b}*} - g_t^{\mathrm{s}*}$ and $g_t^{\mathrm{s}\prime} = 0$. A practical system usually has $Q_t^{\mathrm{b}} > Q_t^{\mathrm{s}} > 0$, so we get $Q_t^{\mathrm{b}} g_t^{\mathrm{b}*} - Q_t^{\mathrm{s}} g_t^{\mathrm{s}*} > Q_t^{\mathrm{b}}(g_t^{\mathrm{b}*} - g_t^{\mathrm{s}*}) = Q_t^{\mathrm{b}} g_t^{\mathrm{b}\prime}$.
2) $g_t^{\mathrm{b}*} < g_t^{\mathrm{s}*}$. Here, let $g_t^{\mathrm{s}\prime} = g_t^{\mathrm{s}*} - g_t^{\mathrm{b}*}$ and $g_t^{\mathrm{b}\prime} = 0$. We have $Q_t^{\mathrm{b}} g_t^{\mathrm{b}*} - Q_t^{\mathrm{s}} g_t^{\mathrm{s}*} > Q_t^{\mathrm{s}}(g_t^{\mathrm{b}*} - g_t^{\mathrm{s}*}) = -Q_t^{\mathrm{s}} g_t^{\mathrm{s}\prime}$.

Both cases imply that $\{g_t^{\mathrm{b}\prime}, g_t^{\mathrm{s}\prime}\}$ costs less in trading energy with the grid than $\{g_t^{\mathrm{b}*}, g_t^{\mathrm{s}*}\}$. As the MISOCP (25) is a cost-minimizing problem, a good solution must satisfy $g_t^{\mathrm{b}} g_t^{\mathrm{s}} = 0$.

If we fix $x_{i,t}^n = 0$ in (23), then we have $p_{i,t}^n = z_{i,t}^n = r_{i,t}^n = y_{i,t}^n = a_{i,t}^n = 0$. Therefore, any solution meeting constraints (16) and (23) also meets $a_{i,t}^{\mathrm{d}} a_{i,t}^{\mathrm{c}} = 0$.

Appendix B
Proof of Proposition 1

Proof: Let $\boldsymbol{Y}_i$ denote the decision vector of battery i with $\boldsymbol{Y}_i \coloneqq \{\boldsymbol{p}_i, \boldsymbol{a}_i, \boldsymbol{r}_i, \boldsymbol{w}_i\}$ where $\boldsymbol{w}_i \coloneqq \{\boldsymbol{y}_i, \boldsymbol{z}_i, \boldsymbol{pr}_i\}$. Define a convex function $h_i(\boldsymbol{Y}_i)$ such that $h_i(\boldsymbol{Y}_i) \leq 0$ holds if and only if $\boldsymbol{Y}_i$ satisfies the constraints of problem (34). Considering the prices $\boldsymbol{\Phi}$ are constants, the KKT conditions of battery i's problem (34) for all $i \in \boldsymbol{I}$ are given by

$$\frac{\partial \varphi_{i,t}^{\mathrm{d}}}{\partial p_{i,t}^{\mathrm{d}}} - \lambda_t + \beta_i^{\mathrm{h}} \frac{\partial h_i}{\partial p_{i,t}^{\mathrm{d}}} = 0, \forall i \in \boldsymbol{I}, t \in \boldsymbol{T}, \tag{40a}$$

$$\frac{\partial \varphi_{i,t}^{\mathrm{c}}}{\partial p_{i,t}^{\mathrm{c}}} + \lambda_t + \beta_i^{\mathrm{h}} \frac{\partial h_i}{\partial p_{i,t}^{\mathrm{c}}} = 0, \forall i \in \boldsymbol{I}, t \in \boldsymbol{T}, \tag{40b}$$

$$\frac{\partial \varphi_{i,t}^{n}}{\partial a_{i,t}^{n}} - \mu_t + \beta_i^{\mathrm{h}} \frac{\partial h_i}{\partial a_{i,t}^{n}} = 0, \forall n \in \{\mathrm{d}, \mathrm{c}\}, i \in \boldsymbol{I}, t \in \boldsymbol{T}, \tag{40c}$$

$$\frac{\partial \varphi_{i,t}^{n}}{\partial r_{i,t}^{n}} - \pi_t^n + \beta_i^{\mathrm{h}} \frac{\partial h_i}{\partial r_{i,t}^{n}} = 0, \forall n \in \{\mathrm{d}, \mathrm{c}\}, i \in \boldsymbol{I}, t \in \boldsymbol{T}, \tag{40d}$$

$$\nabla_{\boldsymbol{w}_i} \sum_{\substack{n \in \{\mathrm{d},\mathrm{c}\}, \\ t \in \boldsymbol{T}}} \varphi_{i,t}^{n} + \beta_i^{\mathrm{h}} \nabla_{\boldsymbol{w}_i} h_i = \boldsymbol{0}, \forall i \in \boldsymbol{I}, \tag{40e}$$

$$\left[\beta_i^{\mathrm{h}}\right] : h_i(\boldsymbol{Y}_i) \leq 0, \forall i \in \boldsymbol{I}, \tag{40f}$$

$$\beta_i^{\mathrm{h}} \geq 0, \quad \beta_i^{\mathrm{h}} h_i(\boldsymbol{Y}_i) = 0, \forall i \in \boldsymbol{I}. \tag{40g}$$

By the market clearing conditions (36), the objective in (35) can be written as

$$\max_{\boldsymbol{g}, r_{\mathrm{m}}} \; Q_{\mathrm{m}} r_{\mathrm{m}} - r_{\mathrm{m}} \sum_{t \in \boldsymbol{T}} \left(\pi_t^{\mathrm{d}} + \pi_t^{\mathrm{c}}\right) + \sum_{t \in \boldsymbol{T}} \left(Q_t^{\mathrm{s}} g_t^{\mathrm{s}} - Q_t^{\mathrm{b}} g_t^{\mathrm{b}}\right) + \sum_{t \in \boldsymbol{T}} \lambda_t \left(g_t^{\mathrm{b}} - g_t^{\mathrm{s}}\right).$$

Considering the prices $\boldsymbol{\Phi}$ are constants, the KKT conditions of the system manager problem (35) are given by

$$-Q_{\mathrm{m}} + \sum_{t \in \boldsymbol{T}} \left(\pi_t^{\mathrm{d}} + \pi_t^{\mathrm{c}}\right) - \beta_{\mathrm{m}} = 0, \tag{41a}$$

$$Q_t^{\mathrm{b}} - \lambda_t - \beta_t^{\mathrm{b}} = 0, \forall t \in \boldsymbol{T}, \tag{41b}$$

$$-Q_t^{\mathrm{s}} + \lambda_t - \beta_t^{\mathrm{s}} = 0, \forall t \in \boldsymbol{T}, \tag{41c}$$

$$[\beta_{\mathrm{m}}] : r_{\mathrm{m}} \geq 0, \tag{41d}$$

$$\left[\beta_t^{\mathrm{b}}\right] : g_t^{\mathrm{b}} \geq 0, \tag{41e}$$

$$\left[\beta_t^{\mathrm{s}}\right] : g_t^{\mathrm{s}} \geq 0, \tag{41f}$$

$$\beta_{\mathrm{m}} \geq 0, \quad \beta_t^{\mathrm{b}} \geq 0, \quad \beta_t^{\mathrm{s}} \geq 0, \forall t \in \boldsymbol{T}, \tag{41g}$$

$$\beta_{\mathrm{m}} r_{\mathrm{m}} = 0, \quad \beta_t^{\mathrm{b}} g_t^{\mathrm{b}} = 0, \quad \beta_t^{\mathrm{s}} g_t^{\mathrm{s}} = 0, \forall t \in \boldsymbol{T}. \tag{41h}$$

One can find that the KKT conditions (40) and (41) combining with the market clearing conditions (36) are exactly the KKT conditions of the SOCP. As $\{\boldsymbol{\Theta}^*, \boldsymbol{\Phi}^*\}$ corresponds

to the optimal KKT point of the SOCP, $\{\boldsymbol{\Theta}^*, \boldsymbol{\Phi}^*\}$ also satisfies (40), (41), and (36). This completes the proof. ■

APPENDIX C
PROOF OF PROPOSITION 2

Proof: Let u_i^* denote the maximum utility of battery i at the market equilibrium when battery i provides the three services. Following Proposition 1-1), u_i^* can be derived from the following problem:

$$u_i^* = \max_{\substack{\boldsymbol{p}_i,\boldsymbol{a}_i,\boldsymbol{r}_i,\\ \boldsymbol{y}_i,\boldsymbol{z}_i,\boldsymbol{pr}_i}} \sum_{t\in\boldsymbol{T}} \big[\lambda_t^*\big(p_{i,t}^{\mathrm{d}} - p_{i,t}^{\mathrm{c}}\big) + \mu_t^*\big(a_{i,t}^{\mathrm{d}} + a_{i,t}^{\mathrm{c}}\big) + \pi_t^{\mathrm{d}*} r_{i,t}^{\mathrm{d}} + \pi_t^{\mathrm{c}*} r_{i,t}^{\mathrm{c}}\big] - \sum_{\substack{t\in\boldsymbol{T},\\ n\in\{\mathrm{d},\mathrm{c}\}}} \varphi_{i,t}^n\big(p_{i,t}^n, a_{i,t}^n, r_{i,t}^n, p_{i,t}^n r_{i,t}^n\big),$$

$$\text{s.t.} \quad \text{Constraints in problem (34)}, \tag{42}$$

where the prices are fixed to the optimal $\boldsymbol{\Phi}^*$. Let u_i^0 denote the maximum utility of battery i when it does not provide any service, which means

$$p_{i,t}^n = a_{i,t}^n = r_{i,t}^n = 0, \forall n \in \{\mathrm{d}, \mathrm{c}\}, t \in \boldsymbol{T}. \tag{43}$$

This leads to $p_{i,t}^n r_{i,t}^n = 0$ from (20). We then have $u_i^0 = 0$ according to the utility function in (42). u_i^0 can be also considered as the optimal objective value of problem (42) with the additional constraint (43). Thus, we readily have $u_i^* \geq u_i^0 = 0$, which means that battery i has a non-negative utility if it provides the three services. This completes the proof.

This conclusion can be generalized to the situations that u_i^* denotes the maximum utility of battery i when it provides some of the three services in the market, that is, battery i has a non-negative utility if it provides at least one of the three services. For example, if battery i only provides load shifting, we add the constraint $a_{i,t}^n = r_{i,t}^n = 0$ in the MISOCP (25), the SOCP, and the individual battery problem (34). Then, the above analysis of problem (42) still holds. ■

APPENDIX D
PROOF OF PROPOSITION 3

Proof: Load shifting: By Appendix A, the optimal solution to the SOCP must have $g_t^{\mathrm{b}*} g_t^{\mathrm{s}*} = 0$. We discuss three cases:

1) $g_t^{\mathrm{b}*} > 0, g_t^{\mathrm{s}*} = 0$. In this case, we have $\beta_t^{\mathrm{b}*} = 0$ and $\lambda_t^* = Q_t^{\mathrm{b}}$ according to KKT conditions (41).
2) $g_t^{\mathrm{b}*} = 0, g_t^{\mathrm{s}*} > 0$. This case has $\beta_t^{\mathrm{s}*} = 0$ and $\lambda_t^* = Q_t^{\mathrm{s}}$.
3) $g_t^{\mathrm{b}*} = g_t^{\mathrm{s}*} = 0$. This case yields $\beta_t^{\mathrm{b}*}, \beta_t^{\mathrm{s}*} > 0$ and $Q_t^{\mathrm{s}} < \lambda_t^* < Q_t^{\mathrm{b}}$.

As per constraint (1), it can be seen that equation (37) holds in each of the above three cases. This proves Proposition 3-1).

Balancing: The proof of Proposition 3-2) is straightforward. Equation (38) follows from constraint (6).

PFC: If $r_{\mathrm{m}}^* > 0$, then we have $\beta_{\mathrm{m}}^* = 0$ from KKT conditions (41). This leads to $Q_{\mathrm{m}} r_{\mathrm{m}}^* = r_{\mathrm{m}}^* \sum_{t\in\boldsymbol{T}} (\pi_t^{\mathrm{d}*} + \pi_t^{\mathrm{c}*})$. Combining with constraints (8), we readily obtain equation (39). Note that (39) still holds if $r_{\mathrm{m}}^* = 0$. This completes the proof of Proposition 3-3). ■

APPENDIX E
DEMAND AND WIND PARAMETERS (KWH)

t	D_t	W_t	t	D_t	W_t
1	541.60	748.20	13	519.62	329.62
2	539.58	714.30	14	527.14	321.15
3	531.85	680.22	15	501.29	312.68
4	505.45	646.10	16	479.48	304.35
5	483.82	585.86	17	477.21	323.58
6	475.22	525.69	18	502.56	342.94
7	475.80	465.45	19	535.42	362.29
8	473.80	429.58	20	553.84	377.73
9	475.57	393.80	21	548.52	393.24
10	477.64	358.10	22	528.67	408.84
11	492.29	348.43	23	523.83	422.59
12	504.17	338.96	24	546.38	409.72

REFERENCES

[1] W. Zhong, K. Xie, Y. Liu, C. Yang, and S. Xie, "Multi-resource allocation of shared energy storage: A distributed combinatorial auction approach," *IEEE Trans. Smart Grid*, vol. 11, no. 5, pp. 4105–4115, Sep. 2020.

[2] N. Y. Soltani and A. Nasiri, "Chance-constrained optimization of energy storage capacity for microgrids," *IEEE Trans. Smart Grid*, vol. 11, no. 4, pp. 2760–2770, Jul. 2020.

[3] W. Zhong, K. Xie, Y. Liu, C. Yang, S. Xie, and Y. Zhang, "Online control and near-optimal algorithm for distributed energy storage sharing in smart grid," *IEEE Trans. Smart Grid*, vol. 11, no. 3, pp. 2552–2562, May 2020.

[4] R. Hollinger, A. M. Cortes, and T. Erge, "Fast frequency response with BESS: A comparative analysis of Germany, Great Britain and Sweden," in *Proc. EEM*, Lodz, Poland, 2018, pp. 1–6.

[5] D. Wu, C. Jin, P. Balducci, and M. Kintner-Meyer, "An energy storage assessment: Using optimal control strategies to capture multiple services," in *Proc. IEEE Power Energy Soc. Gener. Meeting*, Denver, CO, USA, 2015, pp. 1–5.

[6] O. Mégel, J. L. Mathieu, and G. Andersson, "Scheduling distributed energy storage units to provide multiple services under forecast error," *Elect. Power Energy Syst.*, vol. 72, pp. 48–57, Nov. 2015.

[7] R. Moreno, R. Moreira, and G. Strbac, "A MILP model for optimising multi-service portfolios of distributed energy storage," *Appl. Energy*, vol. 137, pp. 554–566, Jan. 2015.

[8] E. Namor, F. Sossan, R. Cherkaoui, and M. Paolone, "Control of battery storage systems for the simultaneous provision of multiple services," *IEEE Trans. Smart Grid*, vol. 10, no. 3, pp. 2799–2808, May 2019.

[9] S. Gupta, V. Kekatos, and W. Saad, "Optimal real-time coordination of energy storage units as a voltage-constrained game," *IEEE Trans. Smart Grid*, vol. 10, no. 4, pp. 3883–3894, Jul. 2019.

[10] R. A. Jabr, S. Karaki, and J. A. Korbane, "Robust multi-period OPF with storage and renewables," *IEEE Trans. Power Syst.*, vol. 30, no. 5, pp. 2790–2799, Sep. 2015.

[11] Q. Xu, T. Zhao, Y. Xu, Z. Xu, P. Wang, and F. Blaabjerg, "A distributed and robust energy management system for networked hybrid AC/DC microgrids," *IEEE Trans. Smart Grid*, vol. 11, no. 4, pp. 3496–3508, Jul. 2020.

[12] A. Kargarian, G. Hug, and J. Mohammadi, "A multi-time scale co-optimization method for sizing of energy storage and fast-ramping generation," *IEEE Trans. Sustain. Energy*, vol. 7, no. 4, pp. 1351–1361, Oct. 2016.

[13] Y. Li, Z. Yang, G. Li, D. Zhao, and W. Tian, "Optimal scheduling of an isolated microgrid with battery storage considering load and renewable generation uncertainties," *IEEE Trans. Ind. Electron.*, vol. 66, no. 2, pp. 1565–1575, Feb. 2019.

[14] Z. Shi, H. Liang, S. Huang, and V. Dinavahi, "Distributionally robust chance-constrained energy management for islanded microgrids," *IEEE Trans. Smart Grid*, vol. 10, no. 2, pp. 2234–2244, Mar. 2019.

[15] W. Xie and S. Ahmed, "Distributionally robust chance constrained optimal power flow with renewables: A conic reformulation," *IEEE Trans. Power Syst.*, vol. 33, no. 2, pp. 1860–1867, Mar. 2018.

[16] B. Geißler, A. Morsi, L. Schewe, and M. Schmidt, "Penalty alternating direction methods for mixed-integer optimization: A new view on feasibility pumps," *SIAM J. Optim.*, vol. 27, no. 3, pp. 1611–1636, 2017.
[17] J. Kang, Z. Xiong, D. Niyato, S. Xie, and D. I. Kim, "Securing data sharing from the sky: Integrating blockchains into drones in 5G and beyond," *IEEE Netw.*, vol. 35, no. 1, pp. 78–85, Jan./Feb. 2021.
[18] X. Huang, D. Ye, R. Yu, and L. Shu, "Securing parked vehicle assisted fog computing with blockchain and optimal smart contract design," *IEEE/CAA J. Autom. Sinica*, vol. 7, no. 2, pp. 426–441, Mar. 2020.
[19] (Feb. 2021). *Réseau de Transport d'Électricité (RTE)*. [Online]. Available: https://www.services-rte.com/en/home.html
[20] Y. Dvorkin, "A chance-constrained stochastic electricity market," *IEEE Trans. Power Syst.*, vol. 35, no. 4, pp. 2993–3003, Jul. 2020.
[21] W. Zhong, S. Xie, K. Xie, Q. Yang, and L. Xie, "Cooperative P2P energy trading in active distribution networks: An MILP-based Nash bargaining solution," *IEEE Trans. Smart Grid*, vol. 12, no. 2, pp. 1264–1276, Mar. 2021.
[22] G. P. McCormick, "Computability of global solutions to factorable nonconvex programs: Part I—Convex underestimating problems," *Math. Prog.*, vol. 10, no. 1, pp. 147–175, 1976.
[23] J. Kronqvist, D. E. Bernal, A. Lundell, and I. E. Grossmann, "A review and comparison of solvers for convex MINLP," *Optim. Eng.*, vol. 20, no. 2, pp. 397–455, 2019.
[24] (Feb. 2021). *Tarif Bleu: Regulated Sale Tariff for Electricity*. [Online]. Available: https://particulier.edf.fr/en/home/energy-and-services/electricity/tarif-bleu.html
[25] (Feb. 2021). *Regelleistung*. [Online]. Available: https://www.regelleistung.net

Weifeng Zhong received the Ph.D. degree in control science and engineering from Guangdong University of Technology, Guangzhou, China, in 2019, where he is currently an Associate Professor. He was a Visiting Scholar with Nanyang Technological University, Singapore, in 2021, and a visiting student with the Hong Kong University of Science and Technology, Hong Kong, in 2016. His research interest lies in optimization, resource allocation, and economics in smart grid.

Kan Xie received the Ph.D. degree in control science and engineering from Guangdong University of Technology, Guangzhou, China, in 2017. He joined the Institute of Intelligent Information Processing, Guangdong University of Technology, where he is currently an Associate Professor. His research interests include machine learning, nonnegative signal processing, blind signal processing, smart grid, and Internet of Things.

Yi Liu received the Ph.D. degree in signal and information processing from South China University of Technology, Guangzhou, China, in 2011. He joined the Singapore University of Technology and Design as a Postdoctoral Researcher. In 2014, he worked with the Institute of Intelligent Information Processing, Guangdong University of Technology, where he is currently a Full Professor. His research interests include wireless communication networks, cooperative communications, smart grid, and intelligent edge computing.

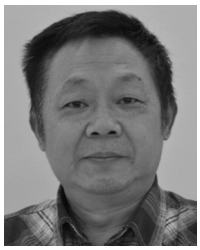

Shengli Xie (Fellow, IEEE) received the B.S. degree in mathematics from Jilin University, Changchun, China, in 1983, the M.S. degree in mathematics from Central China Normal University, Wuhan, China, in 1995, and the Ph.D. degree in control theory and applications from South China University of Technology, Guangzhou, China, in 1997. He is currently a Full Professor and the Head of the Institute of Intelligent Information Processing, Guangdong University of Technology, Guangzhou. He has coauthored two books and more than 150 research papers in refereed journals and conference proceedings and was awarded Highly Cited Researcher in 2020. His research interests include blind signal processing, machine learning, and Internet of Things. He was awarded the Second Prize of National Natural Science Award of China in 2009. He is an Associate Editor for IEEE TRANSACTIONS ON SYSTEMS, MAN, AND CYBERNETICS: SYSTEMS.

Lihua Xie (Fellow, IEEE) received the Ph.D. degree in electrical engineering from the University of Newcastle, Australia, in 1992.

Since 1992, he has been with the School of Electrical and Electronic Engineering, Nanyang Technological University, Singapore, where he is currently a Professor and the Director of Delta-NTU Corporate Laboratory for Cyber-Physical Systems and the Center for Advanced Robotics Technology Innovation. He served as the Head of Division of Control and Instrumentation from July 2011 to June 2014. He held teaching appointments with the Department of Automatic Control, Nanjing University of Science and Technology from 1986 to 1989. His research interests include robust control and estimation, networked control systems, multiagent networks, localization, and unmanned systems. He is an Editor-in-Chief for *Unmanned Systems* and has served as an Editor of IET Book Series in *Control* and an Associate Editor of a number of journals, including IEEE TRANSACTIONS ON AUTOMATIC CONTROL, *Automatica*, IEEE TRANSACTIONS ON CONTROL SYSTEMS TECHNOLOGY, IEEE TRANSACTIONS ON NETWORK CONTROL SYSTEMS, and IEEE TRANSACTIONS ON CIRCUITS AND SYSTEMS-II. He was an IEEE Distinguished Lecturer from January 2012 to December 2014. He is a Fellow of Academy of Engineering Singapore, IFAC, and CAA.